Harvesting of river flow energy for wireless sensor network technology

Ervin Kamenar, Saša Zelenika, David Blažević, Senka Maćešić, Goran Gregov , Kristina Marković, Vladimir Glažar

E. Kamenar, S. Zelenika, D. Blažević, S. Maćešić, G. Gregov, K. Marković, V. Glažar

University of Rijeka

Faculty of Engineering

Vukovarska 58

51000 Rijeka, CROATIA

E-mail: sasa.zelenika@riteh.hr

Phone: + 385 – (0)51 – 651538

Fax: + 385 – (0)51- 651416

E. Kamenar, S. Zelenika, D. Blažević, K. Marković

University of Rijeka

Centre for Micro and Nano Sciences and Technologies

Radmile Matejčić 2

51000 Rijeka, CROATIA

Abstract River courses play a vital role in preserving unpolluted ecosystems. On the other hand, networks of sensor nodes can be used to measure characteristic parameters in the environment such as temperature, pressure, humidity or the concentration of pollutants. In the framework of the EU FP7 project "GOLDFISH", technical competences of a consortium of 11 institutions are hence employed in designing, manufacturing, validating and operating wireless sensors nodes for tracking pollution in remote rivers. The sensor network is composed of sensor clusters located underwater and gateways on the riverbank with long-distance communication links to the central management and monitoring station. Each sensor node is composed of active electronic devices that have to be constantly powered. Batteries can generally be used for this purpose, but problems may occur when they are to be recharged or replaced, especially in the case of large networks placed in scarcely accessible locations. State-of-the-art energy harvesting technologies can hence constitute a viable powering solution. The possibility to use different small-scale river flow energy harvesting principles is thoroughly studied in this work by the University of Rijeka GOLDFISH team: a miniaturized hydro-generator, a 'piezoelectric eel' and a hybrid solution of a rotating shaft plucking a piezoelectric beam. The first two concepts are validated experimentally in a flow channel and in real river conditions. The miniaturized hydro-generator with suitable power management electronics is finally embedded into the wireless sensor node deployed into the river, allowing the GSM transmission of collected data to be successfully performed.

1 Introduction

Tracking of contamination in ecosystems – and remote watercourses in particular – requires an arrangement that continuously monitors the presence of specific chemical agents. Within European Union's 7th framework program, a consortium of 11 partnering institutions from the academic and industrial sectors from Austria, Bolivia, Columbia, Croatia, France, Poland, Slovakia, Sweden and Vietnam has thus set-up a project entitled "GOLDFISH – Detection of Watercourse Contamination in Developing Countries using Sensor Networks – Enlarged". Its aim was to design, manufacture, validate and put into operation an integrated system intended at collecting, processing and transmitting river contamination data to gateways located on the riverbank. Each gateway covers sensor clusters deployed in its communication range and is equipped with long-distance communication links to the central management and monitoring station that processes the data detecting

instantly the presence of contaminating substances in the water (GOLDFISH Description of Work 2013). The foreseen general operating conditions for the GOLDFISH sensor nodes are reported in Table 1.

One of the technological problems related to wireless sensor network technologies is that of enabling autonomous powering of the sensor nodes that are, in fact, miniaturized computing devices designed specifically to perform simpler tasks. The traditional means of powering the sensor nodes is to use batteries that have a limited lifetime. In fact, considering the total foreseen average consumption of a GOLDFISH sensor node of 500 mW (cf. Table 1), a standard 12 V UPS battery with a capacity of 7 Ah would have to be recharged approximately once every 3.5 days. What is more, with such recharging cycles a rechargeable battery would in average last about 7 years. These conditions would constitute a huge challenge, especially in large-area networks deployed in hardly accessible locations. Different energy harvesting principles, especially if coupled with low consumption electronics and suitable power management circuitry, as well as with supercapacitors, represent a way to overcome these restrictions (GOLDFISH Description of Work 2013).

Energy harvesting, relying on various energy conversion principles – from photovoltaics to thermoelectrics, has lately been used in several applications (Erturk 2011, Kazmierski and Beeby 2011, Priya and Inman 2009, Mateu and Moll 2005). Generally, however, the quest for miniaturizing the harvesters, the used energy conversion principles and the considered very specific applications, limit the obtainable power levels of the adopted solutions to the micro- to milli-watts domain (Priya and Inman 2009, Roundy et al 2005, Beeby and Zhu 2015, Kiziroglou et al 2015) which makes them unsuitable for the herein considered case. What is more, small-scale river flow energy harvesting concepts have not yet been comprehensively investigated.

Three energy harvesting concepts, specifically designed for sensor nodes to be placed in watercourses, are thus thoroughly explored in this work: a miniaturized underwater DC hydro-generator, a so-called ‘piezoelectric eel’ and a hybrid turbine solution coupled with a piezoelectric beam (Fig. 1). The corresponding conditioning and management electronics, used to regulate the generated voltage levels and keep them compatible with the foreseen loads, is also designed and optimized (Zelenika et al 2014a).

The developed underwater hydro-generator is optimized via theoretical considerations and preliminary measurements. The optimized configuration is hence tested in controlled conditions in a flow channel as well as in river conditions, allowing hence to establish that the required power levels are achieved. During the final testing phases of the GOLDFISH project, the harvester is thus integrated within the autonomous wireless sensor node in real river conditions.

In the case of the piezoelectric eel, the performed thorough analysis of the optimized eel shapes, positions and bluff body dimensions is presented and discussed. With the aim of determining the achievable power levels, the eels are then prototyped and tested in a flow channel. Preliminary tests in river flow conditions are also performed.

The concept of a hybrid of a rotating shaft and a piezoelectric cantilever, which employs the plucking mechanism proposed by Pozzi and Zhu (2011) for applications in wearable joints, is numerically explored in this work by employing a finite element coupled 3D analysis (Blažević and Zelenika, 2015). To simulate the behavior of this design configuration and obtain the resulting voltage response, a transient analysis is hence performed, allowing to estimate the generated powers.

2 Development of the considered river flow energy harvesting concepts

The miniaturized underwater hydro-generator concept developed in this work is based on a small direct current (DC) generator that is enveloped in a watertight enclosure (Fig. 1 left). On the other hand, the piezoelectric eel (Fig. 1 center) is a composite flag-like compliant device based on piezoelectric polymer, placed in a river stream behind a bluff body. The third concept relies, in turn, on a piezoelectric bimorph cantilever (Fig. 1 right) plucked by plectra protruding from propeller's shaft and then released allowing it to vibrate freely.

2.1 Miniaturized hydro-generator

Although the possibility to use hydro-generators is a well-examined concept on the macro scale, so far it has not been used to power low consumption wireless sensor nodes. The design of the miniaturized hydro-generator in this work (Fig. 2) is based primarily on considerations related to the power levels required by the sensor cluster constituted by the pollution sensors, the respective electronics and the processing unit, as well as on considerations related to the expected river flow conditions in the frame of the GOLFISH project (cf. Table 1). The proposed concept is hence constituted by a DC generator (indicated in Fig. 2 with 1) connected with the propeller shaft (2) via an elastic coupling (3). The diameter of the propeller (4) is optimized to a value of ϕ = 150 mm via MATLAB® simulations based on first-order wind-mill equations reported by Burton et al

(2011), pertinent in the case of incompressible fluids as well. The propeller is connected with the shaft that is centered by using a suitable bearing (5). A radial seal mounted on the propeller's shaft (6) ensures a sealed coupling to the watertight housing (7) that contains slots with silica gel used as desiccant. Two Faulhaber DC generators, whose parameters are listed in Table 2, are employed for the first prototypes. The output powers listed in Table 2 are those given in manufacturer's manual and refer to the mechanical power that can be generated by the device when used in the motor mode, but can roughly be used as an estimate of the achievable maximal power levels when the device is used as a generator, too.

For the sake of determining efficient propeller shapes, a rough verification of turbine blades characteristics is performed prior to experimental investigations via numerical analysis. The Friendship Systems CAESES software is used in this frame to generate the parametric model of the propeller blades. A steady state three-dimensional incompressible fluid flow is considered. It is hence established that, for the highest considered river flow velocities, a maximum pressure value on the propeller blades does not exceed 50 kPa, which is negligible. Based on these simulations, several propeller variants with different number of propeller blades, each with different widths, are thus prototyped. The propellers and the respective watertight enclosure are printed in a first instance on a 3D printer (Fig. 3 and Fig. 4 left). The resulting assembly of the first prototype of the miniaturized underwater hydro-generator harvester is shown in Fig. 4 on the right.

A set of preliminary field experiments using the described prototypes is performed next in real river conditions at the Rječina river near Rijeka, Croatia. The hydro-generator is anchored in close proximity to the river surface. The average velocity of the flow at the river surface is approximately measured by using a piece of Styrofoam thrown into the river and measuring repetitively the time needed to transport it for 10 meters. It is hence established that in the first set of experiments the flow velocity is approximately $v_r = 0.6$ m/s, whereas the river flow velocity at the position of the second set of experiments is about $v_r = 1$ m/s. The Faulhaber 1724006SR DC generator, which can generate up to 6 V, is used (cf. Table 2). Results in terms of the voltage generated by the hydro-generator while using the two propellers of Fig. 3 without electrical loads are approximately the same (see Table 3). Tests with propellers with two blades proved that this configuration is up to 30 % less efficient. In fact, as reported in Burton et al (2011), configurations with an odd number of blades are generally better. On the other hand, it is experimentally assessed that propellers with five blades do not induce meaningful improvements with respect to those with three blades.

Since the generated voltage is lower than that needed to power the foreseen sensors and electronics, in the second set of experiments a Faulhaber 1724012SR DC generator, having a 12 V maximum output voltage (cf. Table 2), is employed. The power management electronics described in Section 3, with a supercapacitor with a C_2 = 5 F capacitance and a "dummy load" composed of 5 LEDs, are used in this set of experiments. At the turbine (i.e. at the input into the system), roughly 10 V and 70 mA, corresponding to a generated power of ca. P_{IN} = 700 mW, are hence obtained. This power level corresponds to that obtained from the mentioned preliminary calculations used in dimensioning the propellers. The corresponding measured output electrical parameters are, in turn, about 4.5 V and 110 mA, i.e. roughly P_{OUT} = 500 mW in one and 3.3 V at 35 mA (P_{OUT} = 115 mW) in the other considered experimental configuration.

Based on the performed field tests, the design of the miniaturized hydro-generator is optimized further (Fig. 5). Due to its good anticorrosive properties, a brass watertight housing is thus foreseen and, to facilitate the mounting procedure, it is split in three parts (indicated in Fig. 5 with 7). The other main components are basically the same (and indicated with the same indexes) as in the original design of Fig. 2. The part indicated in Fig. 8 with 8, made from compliant rubber, is a cable feedthrough. The machined enclosures and all the other elements of the assembly of the resulting optimized miniaturized underwater hydro-generator are shown in Fig. 6. The ϕ = 150 mm propeller is finally printed in the ABSplus (acrylonitrile butadiene styrene) light thermoplastic material on a Stratasys Fortus 250mc 3D printer. In the final design configuration, the underwater hydro-generator has hence overall dimensions of 150 mm x 180 mm.

2.2 Piezoelectric eel

Several concepts for low-level energy harvesting of air or water flows, mainly based on the conversion of flow energy via the direct piezoelectric effect, have been suggested in literature. Solutions based on ceramic piezoelectric cantilevers (Akcabay and Young 2013), ceramic piezoelectric cantilevers with cylindrical extensions (Gao et al 2011), piezoelectric polymer cantilevers coupled with a flexible diaphragm (Wang et al 2012), piezoelectric polymer jellyfish (Wu and Lai 2010) and the piezoelectric polymer eel concept (Allen and Smits 2001, Carrol 2002, Doare and Michelin 2011, Taylor et al 2001, and Techet et al 2002), have been investigated to date in this frame.

In particular, piezoelectric eels, that attained the most attention in the research community, are compliant composite thin structures placed in the furrow of a bluff body located in a fluid flow (Fig. 1 center). Depending on flow velocity and the geometry of the used bluff body, the latter induces von Karman vortex street effects that cause the flapping of the piezoelectric membrane placed behind it. The membrane is hence coerced to flutter in an eel-like motion, thus generating alternating electric charge on the surfaces of the piezoelectric polymer layers. The accumulated electric charge is drained via electrodes covering the piezoelectric surfaces. The resulting voltage can therefore be fed into an energy harvesting/conditioning circuit. The studies of this concept available to date in the literature are limited, however, to the analysis of the solid-fluid interactions and the efficiency of generating the flapping motion of the eels, without a practical determination of the obtainable power levels.

The eel design considered in this work is based on the polyvinylidene fluoride (PVDF) polymer with excellent mechanical and piezoelectric properties (Measurement Specialties 2008). In fact, PVDF is a lightweight engineering plastic with high moisture resistance (< 0.02% moisture absorption) and high flexibility (with elongations of up to $\varepsilon \leq 50$ %) that can be shaped into any design and glued with most commercial adhesives. It is mechanically durable (with a yield strength of $\sigma_{0.2}$ = 55 MPa and Young's modulus of E = 2-4 GPa) and has a high elastic compliance (up to 10 times that of ceramic materials). When compared to other piezoelectric polymers in terms of the piezoelectric coefficient, it surpasses most of them by an order of magnitude ($d_{31} \approx 20$ pC/N), while the usual values of its electromechanical coupling factor κ are around 10%. Additionally, any electrode pattern can be easily deposited onto its surface by employing either sputtering or a screen-printing process.

The available research about the piezoelectric eel concept delineates a strong dependence of the maximum produced voltages on river flow velocity v_r, bluff body shape and size, eel dimensions (including the number of electrode segments) and distance of the eel from the bluff body. It would also seem that an optimal solution, where the vortex shedding frequency matches that of the eel mode shapes, can be obtained only in a very narrow range of these variables. A practical solution that would allow eel's constant fluttering while the sensor cluster is in its sleep mode, thus gathering enough energy for the pollution measurements foreseen in the GOLDFISH project, is hence sought in the framework of the present work. A harvester solution for a variable river flow velocity and a number of designed variables with not-so-strict constraints is thus aimed for. A suitable 2D model of the eel is thus custom-built in C++ by employing the penalty immersed boundary method

(PIBM – Kim and Peskin 2007, Zelenika et al 2014b), wherein fluid flow is modelled using Navier-Stokes equations for an incompressible viscous fluid:

$$\left.\begin{aligned} \rho\left(\frac{\partial \vec{u}}{\partial t} + \vec{u}\nabla\vec{u}\right) &= -\nabla p + \mu\Delta\vec{u} + \vec{f} \\ \nabla\vec{u} &= 0 \end{aligned}\right\} \tag{1}$$

Here t is time, ρ is the density of the fluid, $\vec{u}$ is fluid's velocity, p is the pressure in the fluid, $\vec{f}$ is the external force density, while μ is the viscosity of the fluid.

In PIBM the forces acting along a beam immersed in the fluid are transferred to the fluid

$$\vec{f}(\vec{x},t) = \int_{\mathcal{C}} \vec{F}(s,t)\delta\left(\vec{x} - \vec{X}(s,t)\right) ds \tag{2}$$

while fluid velocity is applied to the beam

$$\frac{\partial \vec{X}}{\partial t}(s,t) = \vec{U}(s,t) = \int_{\Omega} \vec{u}(\vec{x},t)\delta\left(\vec{x} - \vec{X}(s,t)\right) d\vec{x} \tag{3}$$

In the above expressions, $\mathcal{C}$ is the curve that geometrically represents the beam, while Ω is the domain of the fluid, $\vec{x}$ is the space variable, s is the parameter of curve $\mathcal{C}$, $\vec{F}$ is the force density along the beam, $\vec{X}$ is the position of the beam, $\vec{U}$ is the velocity of the beam and δ is the Dirac delta function.

In the herein considered case of the flow behind a bluff body, the force along the beam is defined as:

$$\vec{F}(s,t) = -K_0\left(\vec{X} - \vec{X}_0\right) - R_0\vec{U} \tag{4}$$

where $\vec{X}_0$ is the fixed position of the beam, K_0 is the stiffness of the fictitious springs that are forcing the beam to stay close to the fixed position, while R_0 is a control coefficient that forces the beam to be almost at rest.

In the case of the eel, in the PIBM algorithm a second beam that carries the mass is introduced. The first beam interacts thus with the fluid and is subject to elastic and bending forces, whereas the inertial forces are transferred to the second beam and not to the fluid:

$$\vec{F}(s,t) = \frac{\partial}{\partial s}(\sigma\vec{\tau}) - \frac{\partial^2}{\partial s^2}\left(\frac{c_b}{2}\frac{\partial^2\vec{X}}{\partial s^2}\right) - K\left(\vec{X} - \vec{Y}\right) \tag{5}$$

$$M\frac{\partial^2\vec{Y}}{\partial t^2} = \vec{G}(s,t) = -K\left(\vec{Y} - \vec{X}\right) \tag{6}$$

In the above expressions σ is tension, $\vec{\tau}$ is the unit vector tangent to curve $\mathcal{C}$, c_b is the bending coefficient, $\vec{Y}$ is the position of the massive beam, M is mass, $\vec{G}$ is the force density along the massive beam and K is the stiffness

coefficient of the springs connecting the two beams.

Finally, the inextensibility condition must be explicitly stated as:

$$\frac{\partial \vec{X}}{\partial s} \cdot \frac{\partial \vec{X}}{\partial s} = 1 \tag{7}$$

and tension must be found from the derived equation.

Based on the described model, the voltage *V*, resulting from the motion of the piezoelectric membrane, can be evaluated as:

$$\frac{dV}{dt} = \alpha V + \beta \int_0^l \frac{dc}{dt} |\vec{\tau}| ds \tag{17}$$

where α and β are coefficients that depend on the characteristics of the used piezoelectric material, while c is the curvature of the eel.

The described 2D model is hence used to simulate the formation of the von Karman vortex street occurring in the furrow of the bluff body, as well as the interaction of the vortices with the piezoelectric membrane (Fig. 7 left). Based on this model, a preliminary optimization of eel's shape, position and bluff body dimensions, at a chosen river flow velocity of v_r = 1 m/s, where the objective function is maximizing eel's voltage output, is performed by employing the GoSUMD software by AIMdyn Inc. GoSUMD is a software tool that enables a simultaneous examination of global uncertainties and global contributions of a large number of uncertain parameters on the outputs of interest. It is based on some of the fastest available computational algorithms for nonlinear model representation and sampling (AIMdyn Inc. 2015). In the considered eel's concept case, the optimization is performed by using the mesh adaptive direct search algorithm for mixed variables proposed by Abramson et al (2009).

The optimization is performed in two runs: in the first run, four electrode segments are considered regardless of the length of the eel, while in the second run fixed length (5 cm) electrode segments are placed along eel's length. The input parameters chosen for the optimization runs are the length *L* of the eel, the radius *R* of the tubular bluff body and the distance *d* of eel's clamped end from the bluff body (Fig. 7 right). During the optimization runs, the parameters are chosen in the following ranges (expressed in meters): $L \in [0.20, 1.00]$, $R \in [0.05, 0.2]$, $d \in [0.02, 0.15]$ in the first optimization run, and $L \in [0.20, 1.00]$, $R \in [0.1, 0.3]$, $d \in [0.05, 0.2]$ in the second run. What is more, all model input parameters have continuous uniform distributions and one hundred quasi-random samples are chosen in each run in the range of input parameters; the resampled

points are obtained by using the permutations of the original sample. To speed up the fluttering process, in both runs the eel is set into a pre-bent shape prior to the beginning of the simulation. The investigated physical system is then simulated in a 0.1 s period, with an average computational time of 3 h per sample. After the model is learnt, sensitivity analyses are performed by using derivative and variance sensitivity methods. As a result, in the first run the highest influencing indices are obtained for length *L*, while radius *R* has a lower influence and distance *d* the lowest. In the second run, parameter *L* is still the most influential, followed, however, by *d* and only then by *R*, with an order of magnitude difference between the influence of *L* and of the other two parameters. The interrelated contribution of the input parameters is also to be considered. It is thus established that in the first optimization run the *d*-*L*, *d*-*R* and *R*-*L* relations are important, as are the *d*-*L* and *R*-*L* interconnections in the second run. Finally, for the first run the optimal values for *R*, *L* and *d* are established as: 0.2 m, 0.24 m, and 0.02 m, while for the second run the optimal values are, respectively, 0.21 m, 0.46 m and 0.2 m (AIMdyn Inc. 2015).

Since the models allowed constraining the domain of values of eel's design parameters, of bluff body dimensions and of the distances between the bluff body and the eel, aimed at maximizing the respective output voltages, a prototype eel could be designed so as to gain insight into the dynamics of the investigated device. Eel's design, modified in cooperation with the company Measurement Specialties chosen for its manufacture, with the aim of selecting the most effective substrate material, electrode pattern and watertight encapsulation, is thus depicted in Fig. 8. The assembly (Fig. 8 left) consists thus finally of 13 layers:

- a central substrate Mylar® layer (t_s = 125 μm) – designated in Fig. 8 left with 1;
- two active piezoelectric PVDF layers (t_{PVDF} = 110 μm) annealed at 60 ˚C and plasma etched to ensure better adhesion of the electrodes – designated with 3;
- four ultra-thin screen-printed conductive silver ink electrode layers in an arrangement of totally 16 electrodes (8 positive and 8 negative) – designated with 2 (see also Fig. 8 right);
- two outer protective Mylar® layers (t_p = 25 μm) that ensure a watertight enclosure of the device – designated with 4,
- and four pressure sensitive epoxy layers (t_{ep} = 10 μm) applied between the PVDF and the Mylar® layers.

The manufactured prototype, having a total length of *L* = 621 mm and costing ca. 700 € per piece in a small series production, is shown in Fig. 9 left where the four silver ink electrode pattern is clearly visible. As shown in Fig. 8 on the right and in Fig. 9 on the left, to ensure charge collection at the most convenient location, each

of the 16 electrodes (four electrodes on each side of the two PVDF layers) requires a collector (drain) leading out to one of the solder tab crimped contacts at the clamped end of the eel. Due to the space needed to place the drains, the actual eel's assembly is wide and measures w = 194 mm. A potentially bigger number of electrode segments would further increase eel's width and make the device somewhat impractical when considering the needed electric connections but, on the other hand, it would also probably increase the obtained powers due to a smaller rate of potential voltage cancelations owing to the fluttering shapes of the eel during its operation (see also below). What is more, although the nominal device thickness is $t_T \approx 435$ μm, the actual thickness measured on the manufactured prototypes by using a stereomicroscope (Fig. 9 right) is in average around 450 μm. This is due to the manufacturing tolerances on the thickness of the various layers constituting the eel as well as the irregularities (partial delamination and captured air bubbles) that occurred during the manufacturing process.

The availability of the prototypes allows also measuring the Young's modulus of the eel assembly, which is needed for tuning the numerical models and for interpreting correctly the experimental measurements. For this purpose, a universal Shimadzu Autograph AGS-X tensile machine, available at the Laboratory for Precision Engineering and Micro- and Nanosystems Technologies of the Centre for Micro- and Nano-Sciences and Technologies of the University of Rijeka, Croatia, is employed. The testing machine is equipped with a 5 kN load cell having a resolution of 10 N, while the resolution of the respective extension measurement device (i.e. of the elongation ε of the sample) is 10 μm. One of the prototype eels is hence sacrificed and cut into 250 x 25 mm strips that are placed between the wedge grips of the tensile machine. A static load test is performed allowing to determine, as shown in Fig. 10, that the composite eel's material exhibits a linear stress-strain behavior up to $\sigma_{0.2} \approx 40$ MPa with a Young's modulus of E ≈ 3.5 GPa. It is also established that the ultimate tensile strength of the eel is at about $\sigma_M \approx 186$ MPa.

2.3 Propeller's shaft plucking a piezoelectric beam

The third concept proposed for harvesting river flow energy in the framework of the GOLDFISH project, is based on a piezoelectric cantilever bimorph periodically 'plucked' (i.e. struck) by plectra mounted on the shaft of a turbine (Fig. 1 right). The cantilever is hence allowed to vibrate freely thus converting, via the direct

piezoelectric effect, its transient mechanical response into electric charge. In the conceived configuration, the cantilever is clamped on the inner side of the housing of the hydro-generator and orientated perpendicular to the rotation axis of the shaft that hosts several plectra protruding radially (Fig. 1 right and Fig. 11).

A first-order approximation of the power obtainable from the transient response of a piezoelectric bimorph cantilever can be studied numerically by employing finite element modelling (FEM) and considering a single impact of the plectrum inducing a deflection δ of the cantilever. Assuming that the geometry of the propeller of the hydro-generator is that described in section 2.1 and that the river flow speed is v_r = 1 m/s, a rotational frequency of 250 rpm is obtained (cf. also Fig. 16 right). An off-the-shelf Midé Technology® Volture V21b energy scavenger is thus considered (cf. in this regard Blažević and Zelenika 2015 and Midé Technology Corp 2009). The respective maximum dynamic tensile strength of the PZT-5A ceramic piezoelectric layers, that delimits the maximum allowable deflection δ_{max} of the cantilever, is σ_{M_dyn} = 27.6 MPa. Simple strength of materials first-order calculations can hence be employed, allowing to determine the resulting admissible forces to be applied at the free end of the cantilever. Taking into account a 20 % safety factor, a value of F_{max} = 0.765N is obtained, thus implying a δ_{max} =0.32 mm maximal deflection (Fig. 11). Given this value and considering the rotational frequency of shaft's axis, an approximate impact time, during which the plectrum is in contact with the cantilever, can be calculated to be $t_i \approx 0.35$ ms.

A FEM simulation is thus set-up in the ANSYS® software package (Fig. 12 left) as a transient analysis that is thoroughly described and experimentally verified by Blažević and Zelenika (2015). In this particular case, the excitation profile at the free end of the cantilever is modelled by using MATLAB® as a ramped load F_{max} lasting exactly throughout the duration of the calculated impact time t_i. The load is then instantly released inducing the free vibration transient response of the cantilever (Fig. 12 right). In the used model, the piezoelectric layers are connected in a series electrical circuit coupled with an R_l = 100 Ω resistor. This value is chosen so as to simulate the internal electrical resistance of the downstream elements of the system (i.e. of the used power management electronics described in section 3).

Results of the performed simulations allow establishing that a scant ($U \approx 0.27$ V) voltage is generated from the single impact on the piezoelectric beam. This value cannot allow overcoming the threshold voltage limit required for the supply of energy to the management electronics described in the following section. Further numerical and experimental investigations, considering several plectra and the inclusion of a larger number of

piezoelectric cantilevers being concurrently struck by the protrusions on the shaft of the turbine, are hence planned, although the results of the studies and experiments reported by Pozzi et al (2015) would seem to indicate that these configurations do allow obtaining high voltage levels, but are limited in terms of maximal output powers to few mW, i.e. still far from sufficient for the herein considered case.

3 Power management electronics

By employing the hydro-generator, DC voltage, with an amplitude dependent on river flow velocity, is generated. On the other hand, the piezoelectric eel and the hybrid energy harvesting concepts generate random voltage amplitudes. The obtained energy must therefore be properly managed to achieve DC voltage levels compatible with the used sensors and the respective electronics (Zelenika et al 2014a). The main purpose of the necessary electrical circuitry is hence to reduce and stabilize the voltage levels to a value of 5 V (or, alternatively, 3.3 V) to be used for powering the electronics of the sensor cluster. What is more, the electronics is also aimed at storing excessive energy on a supercapacitor so that it can be used as a power source when the communications module requires higher power bursts.

There are several commercially available energy harvesting chips that can be used to achieve this functionality. The chip's input voltage, depending on its type, can be in the range from few mV up to several tens of V. In this regards, additional passive elements (resistors, capacitors and inductors) have to be added and optimized in order to efficiently use the harvested energy, as well as to ensure undisturbed operation of the connected loads (Zelenika et al 2014a). In the framework of the present work, a power management electronics based on a Fujitsu Semiconductor integrated circuit is hence designed, manufactured and used in all the performed flow channel and field experiments. The list of the used electrical elements is given in Table 4, while the electrical scheme and the manufactured PCB are shown in Fig. 13.

It is to be noted here that the harvester is to be integrated within a sensor node system that has a backup UPS battery. Internal sensor node logic switches then the battery on and off depending on energy production (by the harvester) and energy consumption. When the battery is triggered, the supercapacitor is charged to 4.6 V; the battery is hence switched off. From that point on, the discharging of the supercapacitor is replenished by the charge produced by the used harvester throughout the period when the voltage on the supercapacitor is above

3.6 V. Only when the voltage drops below this threshold, i.e. when the energy generated by the harvester is not sufficient to cover consumption, the battery is turned on again topping-up the lack of energy given by the difference of that produced by the harvester and that drawn by the electrical loads.

4 Measurements in controlled flow conditions in a flow channel

Based on the above consideration, experiments in a flow channel are set-up for the miniaturized DC hydro-generator and the piezoelectric eel energy harvesting concepts. An experimental flow channel with suitable dimensions, that enables controlled variations of water flow velocities while allowing for concurrent measurements of the voltages produced by the harvesters, is available at the Naval Research Institute in Zagreb, Croatia. The test segment of the channel is 2.2 m long, while its active cross-section is 0.5 x 0.5 m. It is suited to produce computer controlled maximal flow velocities of up to 8 m/s with increments of 0.25 m/s. Appropriate interfaces for the considered harvester test beds and the electrical feedthroughs leading out of the chamber are prepared by the staff of the Institute. The wings-based sensors of hydrometric screw turbines are used to attain stable measurements of water flow velocities; one sensors is thus mounted at the beginning of the test segment and one at its end. All the control and regulation components of the Institute's system are then interfaced to an apposite National Instruments data acquisition system.

4.1 Measurements on the miniaturized hydro-generator harvester

Based on the performed preliminary field measurements, a set of experiments is hence performed in the described flow channel on the optimized assembly of the hydro-generator described in section 2.1 (Fig. 14). The miniaturized hydro-generator is hence fixed to the flow channel via a suitable support and tested within a flow velocity range continuously increased up to v_r = 4 m/s in a relatively short time span.

In a first set of measurements, the Faulhaber 1724012SR generator considered in section 2.1 is used again. On the other hand, the foreseen electrical load is simulated via a 'dummy load' constituted by 10 LED diodes; for the 5 V set-up, R = 150 Ω resistors are used, while for the 3.3 V arrangement R = 68 Ω resistors are used. The scheme of the overall used measurement set-up is hence given in Fig. 15.

The measurements are performed as follows:

1. The water flow velocity is increased continuously from 0 to a value at which the propeller starts to rotate. The respective rpm velocity of the propeller is measured by using a stroboscopic device.
2. The velocity is increased continuously from the above value to a value when the supercapacitor on the power management electronics starts charging.
3. The water flow velocity is further increased and the measurements are performed without and with electrical loads. The time needed to charge and discharge the capacitor is concurrently monitored.
4. The maximum admissible flow velocity is achieved when the maximum voltage at the generator is reached.
5. Cyclic tests are used to verify the repeatability of the results.

A typical set of obtained results is hence shown in Table 5. It can thus be observed that, within the accuracy of the measurements of the velocity of the propeller, the measured no-load voltage is close to the nominal one. The generated power is again, as during the preliminary measurements on the Rječina river, at the level of about P_{IN} = 700 mW, i.e. it corresponds to calculated values, while the output powers are up to P_{OUT} = 220 mW. The first set of measurements in the flow channel allowed also confirming that, since the voltage generated by the hydro-generator increases with the third power of the flow velocity (Zelenika et al 2014a), it is not possible to cover the wide foreseen range of water flow velocities with a single miniature DC generator. Five Faulhaber generators of the same type, but with different gearheads, are thus considered as a viable solution. With respect to the conditions present during the foreseen field operation in rivers (cf. Table 1), the Faulhaber 2233B018S generator is chosen and it is coupled with gearheads appropriate to cover specific ranges of the overall flow velocities (i.e. guaranteeing that the generator will be rotating in the vicinity of its nominal no-load speed of n_0 = 9000 rpm). The characteristics of the hence adopted configurations are thus listed in Table 6.

Although the nominal voltage of the chosen generator is U_n = 18 V, in a further set of measurements performed at the Naval Research Institute with the final hydro-generator configuration, much higher voltages are purposely produced to attain the voltage vs. flow velocity dependence in the entire considered velocity range (Fig. 16 left). The obtained characteristic can in any case be easily scaled up or down depending on the gearhead mounted on the generator. The corresponding dependence between water flow velocity and rotational speed of the propeller is in turn shown in Fig. 16 right.

The performed measurements allow also establishing that propeller rotation starts at water flow velocities

higher than v_r = 0.59 m/s and then stops when the velocity drops below v_r = 0.37 m/s. This behavior is related to the Stribeck frictional effect: once the static friction torques at the motor windings, bearings and other components is overcome and rotation starts, the torque needed to perpetuate rotation drops to a value related to dynamic friction. Obviously, the flow velocity threshold at which the propeller starts to rotate depends also on the propeller type. The same experimental set-up allows, in fact, confirming that, when the propeller with wider blades, i.e. with a larger effective area, is used, its rotation is initiated at lower flow velocities.

Most importantly, the final set of measurements at the Naval Research Institute's facilities allows confirming that the developed hydro-generator harvester enables generated power levels at the turbine (i.e. at the input into the harvester system) of up to $P_{IN} \approx 1.5$ W. On the other hand, the measured voltages and currents on a 'dummy load' composed of successfully powered LEDs (simulating the sensors cluster) correspond to generator's output powers of up to $P_{OUT} \approx 800$ mW.

4.2 Measurements with the piezoelectric eel harvester

To assess the piezoelectric eel's dynamic behavior and to determine the range of eel's design parameters that would enable its operation in real river conditions, following the piezoelectric eel calculations and prototyping effort thoroughly described in section 2.2 of this work, experiments are performed at the Naval Research Institute's flow channel described above. Four variables, consistent also with those considered in the optimization calculations, are particularly monitored as the most relevant ones: bluff body shape, its size, distance of the eel from the bluff body and flow speed. A suitable test bed, allowing bluff body exchange and repositioning of the eel, is hence designed and manufactured (Fig. 17 left). Two shapes of bluff bodies are used, each with three different widths: tubular bodies with external diameters of ϕ = 100, 150 and 200 mm and plates with W = 100, 150 and 200 mm widths. Three considered eel-to-body distances are, in turn: d = 40, 80 and 120 mm, while the water flow speed is varied in the range v_r = 0.5-2 m/s with 0.5 m/s increments.

With the aim of producing high electric currents, the electrodes of each of the segments of the manufactured eel (depicted in Fig. 8 and Fig. 9) are separately connected in a parallel electrical circuit, i.e. the top outer electrode is connected with the inner bottom electrode, while the top inner electrode is connected with the outer bottom electrode of the segment. In fact, since, as previously stated, the PVDF material can produce high electric charges, a series connection is not necessary, while high currents, which may enable a more efficient

functioning of the downstream electrical loads, are aimed for. The soldered connections at eel's end are then protected from the water by using a two-component epoxy resin. Each of the four parallel connections is in turn attached to an oscilloscope via the electrical feedthrough leading out from the top window of the flow channel. The piezoelectric eel has in any case to be taken out of the flow channel for each measurement run by employing a portal crane, so as to enable the altering of bluff bodies and/or of eel's positions (Fig. 17 right).

280 AC RMS voltage measurements are finally performed by employing the described set-up, with additional repeatability checks of the values at certain flow velocities. In general, in the case of measurements with the eels, the flow channel proved to be too narrow, especially when larger bluff bodies are used with flow velocities $v_r \geq 1.5$ m/s, thus hindering the occurrence of regular von Karman vortexes. This is especially noticeable when plate-shaped bluff bodies are used, inducing a substantial under-pressure just behind them that causes the eel to twist and bend back towards the bluff body, eventually breaking down. The largest experimentally obtained voltages are hence achieved in the water flow velocity range $v_r \approx$ 1-1.5 m/s when the largest tubular bluff body $\phi = 200$ mm, at a distance from the fixed end of the eel of $d \approx 100$ mm, is used. The oscillatory shape of the eel in this condition is quasi-sinusoidal (Fig. 18). As a general trend, it is also observed that for smaller tubular bluff body diameters the eel has to be moved slightly back towards it.

It is to be noted here that the experimentally obtained optimal configuration seems to be in contradiction with the results of the numerical model of section 2.2, indicating that additional comparative analyses are needed. In this regard, part of the discrepancies might be related to the limited simulation time of the numerical model (0.1 s – constrained by overall computing times), that is too short to capture the complete fluttering period of the eel. In fact, the experimentally seen fluttering frequencies are in the 1-3 Hz range.

A more exhaustive examination of the highest experimentally produced voltages is possible by observing the diagrams of Fig. 19. The case of the $\phi = 200$ mm tubular bluff body at three distances d and four flow velocities v_r (bearing in mind that the data for $v_r \approx 2$ m/s are not reliable due to the vicinity of the walls of the flow channel), is displayed. It is thus evident that the highest voltages are produced, longitudinally, in the 2nd (S2) and 3rd (S3) eel's segments of Fig. 9 left, with a comparable voltage magnitude also in the 4th segment (S4). On the other hand, the 1st segment (S1) is basically inactive, which can be attributed to the clamping of the eel at this end. This might, in turn, indicate that a configuration where the eel has a certain degree of rotational freedom at its clamped end would facilitate larger deformations of the S1 segment, thus generating larger voltages in this section as well. The polynomial curves shown in Fig. 19 represent the 'quasi steady state' eel's

shapes achieved while measuring the voltages at the corresponding water flow velocities.

In any case, the resulting maximal experimentally attained AC output RMS voltages for the whole eel reach $U_{max} \approx 30$ V. Based on the resulting charging periods of the supercapacitor, the corresponding output power can be estimated to be in the $P_{OUT} \approx 10$ mW range. The overall power could ultimately be increased by using several eels (i.e. a 'farm' of them – see section 5.1 below).

5 Field measurements in river flows

5.1 Measurements with the piezoelectric eel harvester

Based on the flow channel measurements on the eels described in section 4.2, a suitable set-up for measurements in real river flow conditions is conceived. The resulting test-bed, shown in Fig. 20 left, allows up to four eels to be concurrently mounted, thus enabling the above-mentioned 'farm' configuration to be tested. As during the Naval Research Institute experiments it was established that the fixture of the eel hinders the bending of its S1 section, in this case a rotational degree of freedom at the clamping of the eels is foreseen. Again, both tubular and plate bluff bodies of up to 200 mm can be accommodated in front of the eels, while the frame is anchored to the riverbed by using suitable concrete weights. Regarding electrical connections, initial lab tests are carried out varying the type of connection (parallel and serial) of the sections of each eel, as well as of the connection among the eels. As in the case of the set-up used during the flow channel measurements, all the electrodes of each of eel's segment (S1, S2, S3 and S4) are separately connected in a parallel electrical circuit. On the other hand, as confirmed by initial laboratory tests and MATLAB® simulations, the best results are obtained when the homologous (equally numbered) sections of each eel (i.e. all sections S1, all sections S2, …) are connected in series. It is, in fact, known that this configuration prevents the possibility of one section of the ell electrically feeding another one, which would produce smaller voltages. On the other hand, this configuration enables the voltages to add up. As shown in Fig. 20 right, all the sections of all the four eels are, in turn, finally connected in parallel, since it is experimentally established that this configuration allows the highest overall currents (i.e. powers) to be obtained.

River experiments are then conducted at the Rječina river in the vicinity of Rijeka, Croatia. The surface flow

velocity at the position of the experiments is measured to be approximately $v_r \approx 0.9$ m/s, i.e. smaller than the velocities that allowed achieving the best results in the flow channel. For this reason, the largest bluff bodies are adopted. The depth of the river and the access to the location where the experiments are performed were far from optimal, but meaningful conclusions can nonetheless be drawn based on the executed measurements. All the performed experiments show, in fact, that the enabled rotation of eels' fixtures induces a meaningful improvement of the voltages produced in the S1 sections of the eels with respect to those achieved during the measurements in the flow channel. The voltages in the other eels' segments follow in general the overall trends seen already in the flow channel, with the S2 and S3 segments generating the highest voltages, while the voltages in sections S4 are lower.

Experiments with a $W = 200$ mm wide plate bluff bodies at a $d = 110$ mm distance from the eels allow good von Karman vortexes to be generated and, in the best cases, voltages of up to $U_{max} \approx 70$ V (with average voltages in the range of $U_{av} \approx 30$ V) to be achieved. However, in this case the eels fluttering tends at times to become erratic and generally the eels tend to bend completely to the left or to the right.

When, in turn, $\phi = 200$ mm tubular bluff bodies are employed, the dynamics of eels' fluttering induced by the generated von Karman vortex street is more regular and, as in the case of the performed flow channel experiments, quasi-sinusoidal eel oscillations are obtained. On the other hand, however, the obtained voltages are smaller ($U_{max} \approx 25$ V) than those obtained with the plate-shaped bluff bodies.

In any case, in terms of obtainable powers the river field measurements seem consistent with the results obtained in the flow channel, since a 'farm' of four eels, coupled with the power management electronics described in section 3, allows obtaining maximal output powers in the range of $P_{OUT} \approx 40$ mW.

The executed field experiments confirm, thus, that the eel harvester concept in the studied configurations does not allow to achieve the power levels aimed for in the frame of the GODLFISH project, but could potentially power an underwater sensing device if ultralow power wireless communication devices and low power control electronics could be employed. The study of this pioneering concept will in any case be continued both theoretically and experimentally.

5.2 Measurements on the miniaturized hydro-generator harvester and its integration into the wireless sensor

cluster

River-flow field experiments are ultimately carried out with the final configuration of the developed miniaturized DC hydro-generator energy harvester described in section 4.1, i.e. the one guaranteeing the highest energy production, at three different rivers, the Rječina river near Rijeka, Croatia, the Liewec river near Warsaw, Poland and the Coello river near Ibague, Columbia. The respective conditions during field measurements are reported in Table 7.

During the measurements on the Rječina river, it is confirmed that the proposed configuration of the miniaturized underwater hydro-generator, together with the designed power management electronics, can continuously ensure the needed power levels to sustain the foreseen sensors and electronics and, concurrently, charge the supercapacitor.

Further river flow field experiments are conducted next at the Liewec river in Warsaw, Poland, where the miniaturized hydro-generator harvester is integrated with the actual underwater contamination monitoring system developed by the other GOLDFISH project consortium partners (Fig. 21). In this case, the river flow is precisely measured at the position of harvester's deployment by employing a water stream flow-rate current meter. During all the measurements performed in Poland, the measurement and controller boards are set, according to the design cycle, to collect the data from the sensors every 15 s, while the time needed for the measurements is one second. On the other hand, the communications module used to deliver the data to the gateway located on the riverbank needs a little less than 2 minutes to successfully transmit the data and is set to operate once every hour (cf. also Table 1). It could thus be shown that, for the defined working periods and without using a battery, the miniaturized hydro-generator harvester can successfully power the control and measurement boards, accomplishing thus the main goal of the project. However, since the river flow velocity at the position of the experiments is an essential boundary condition for the developed harvester, and in the Liewec river the flow velocity was barely above the threshold when the propeller rotation starts (cf. section 4.1), it could not yet be unquestionably confirmed that the charging of the communications module, attained during its sleep mode, can withstand its transmission activity.

In order to definitely exclude this last doubt, a final set of field measurements with the integrated sensor node system are conducted at the Coello river, Ibague, Colombia, where the integrated underwater contamination monitoring system will be finally operated. As reported in Table 7, this location is characterized by flow

velocities well above the threshold guaranteeing the most efficient performances of the hydro-generator harvester. What is more, the support of the hydro-generator is modified in these last tests so as to allow a degree of freedom on the yaw of the generator, permitting to achieve an exact alignment of the longitudinal axis of the generator with the direction of the river flow, guaranteeing thus its optimal operation.

The field tests in Columbia allow thus finally undoubtedly confirming that the whole cluster can be successfully powered by employing the developed hydro-generator harvester. In fact, as shown in Fig. 22, after connecting the harvester and deploying the sensor node into the river flow, the power generated by the harvester (oscillating line in Fig. 22) allows guaranteeing a constant voltage output from the supercapacitor (~ 4.6 V) without the need to use the battery. The GSM transmission started at 21:11:04 could thus be successfully performed.

6 Conclusions and outlook

The conception, modelling, calculation, design, manufacturing and validation of the performances of energy harvesting devices to be employed as a power source for pollution monitoring wireless sensor clusters deployed in river streams, is described in this work. Three energy harvesting concepts are proposed: a miniaturized hydro-generator, piezoelectric eels and a hybrid solution of protrusions from a rotating shaft coupled with a piezoelectric cantilever. Advancing on previous work reported in literature, in this work a thorough theoretical and experimental elaboration of these concepts allows determining the attainable power levels and thus evaluating their potential employment in the foreseen application. Comprehensive analytical and numerical analyses are hence performed to optimize the design of the foreseen harvesting devices. The respective power management electronics is also conceived and assembled. The underwater hydro-generator and the piezoelectric eel concept are subsequently validated via functional measurements.

Preliminary experiments in real river conditions performed on the developed hydro-generator allowed establishing that roughly up to $P_{IN} \approx 700$ mW can be generated. Based on these measurements, the design of the harvester is optimized and a further set of measurements is carried out in controlled flow conditions in a suitable flow channel at the Naval Research Institute in Zagreb, Croatia. Besides establishing operational performance data, these measurements allowed input powers of up to $P_{IN} \approx 1.5$ W and output powers of up to

$P_{OUT} \approx 800$ mW, which correspond to calculated values, to be generated. A 'dummy load' composed of LEDs, simulating the sensor cluster, has therefore been successfully powered.

On the other hand, the pioneering piezoelectric eel concept is successfully prototyped. Material tests are performed, followed by dynamics tests performed at the mentioned facilities of the Naval Research Institute. It is thus demonstrated that a single eel behind a $\phi = 200$ mm tubular bluff body can generate up to $P_{OUT} \approx 10$ mW. This overall configuration seems, however, to be somewhat in contradiction with the results of the numerical model, which is probably related to the limited simulation times. On the other hand, a significant limitation during the performed experiments is the small width of the flow channel that induces unwanted boundary effects. Preliminary measurements in a river flow at the Rječina river near Rijeka, Croatia, allowed confirming that a tubular bluff body allows a more regular quasi-sinusoidal response even for a set (i.e. 'farm') of eels, but that the resulting powers are still too low for the foreseen application. In any case, the study of this concept will be continued from both the theoretical and the experimental point of view.

In the final stages of the work, the hydro-generator harvesting device and its power management electronics are successfully tested in real river-flow conditions in three different river courses. The harvester is hence integrated into the sensor node cluster allowing, during field measurement, successful powering of the measurement and controller boards triggered every 15 seconds to collect data from the sensors. The harvester and its power management electronics are consequently embedded into the final configuration of the autonomous sensor network constituted by the sensors, the conditioning electronics, the transceivers and the gateways, which is integrally experimentally validated at the Coello river in Ibague, Columbia. The hydro-generator allowed in this frame the whole sensor cluster to be successfully powered.

Acknowledgements The work presented in this paper was part of and supported by the EU FP7 ICT-2009.9.1 project no. 269985 "GOLDFISH – Detection of Watercourse Contamination in Developing countries using Sensor Networks – Enlarged". The work was partly made possible also by using the equipment funded via the EU European Regional Development Fund (ERDF) project no. RC.2.2.06-0001: "Research Infrastructure for Campus-based Laboratories at the University of Rijeka (RISK)".

References

Abramson MA, Audet C, Chrissis JW, Walston JG (2009) Mesh adaptive direct search algorithms for mixed variable optimization. Opt Letters 3(1): 35-47

AIMdyn Inc. (2015) Report on the sensitivity and optimization results obtained by the GoSUMD software to maximize the produced voltage by piezoelectric eel. AIMdyn Inc., Santa Barbara

Akcabay DT, Young YL (2013) Hydroelastic Response and Energy Harvesting Potential of Flexible Piezoelectric Beams in Viscous Flow. Phys Fluids 24: 054106

Allen JJ, Smits AJ (2001) Energy harvesting eel. J Fluids Struct 15(3-4): 629-640

Beeby SP, Zhu D (2015) Vibration energy harvesting: fabrication, miniaturisation and applications, Proc SPIE 9517A: 9517031-9517038

Blažević D, Zelenika S (2015) Nonlinear numerical modelling and experimental validation of multilayer piezoelectric vibration energy scavengers. Proc SPIE 9517A: 95171F1-5171F13

Burton T et al (2011) Wind Energy Handbook - 2nd ed. Wiley, New York

Carrol CB (2002) Energy harvesting eel. US Patent 6,424,079 B1

Doare O, Michelin S (2011) Piezoelectric coupling in energy-harvesting fluttering flexible plates: linear stability analysis and conversion efficiency. J Fluids Struct 27(8): 1357-1375

Erturk A, Inman D (2011) Piezoelectric energy harvesting. Wiley & Sons, Chichester

Gao X, Shih W-H, Shih WY (2011) Flow Energy Harvesting Using Piezoelectric Cantilevers With Cylindrical Extension. IEEE Trans Ind Electr 60(3): 1116-1118

GOLDFISH (2013) Detection of Watercourse Contamination in Developing Countries using Sensor Networks – Enlarged, Annex I – Description of Work. EU FP7 ICT-2009.9.1 project no. 269985

Kazmierski T, Beeby S (ed) (2011) Energy Harvesting Systems: Principles, Modeling and Applications. Springer, New York

Kim Y, Peskin CS (2007) Penalty Immersed Boundary Method for an Elastic Boundary with Mass. Phys Fluids 19: 053103

Kiziroglou ME et al (2015) Scaling of dynamic thermoelectric harvesting devices in the 1-100 cm^3 range. Proc SPIE 9517A: 95172F1-95172F8

Mateu L, Moll F (2005) Review of Energy Harvesting Techniques and Applications for Microelectronics. Proc

SPIE 5837: 359-373

Measurement Specialties (2008) Piezo Film Sensors Technical Manual. Measurement Specialties, Hampton

Midé Technology Corp (2009) Volture Products Spec Sheet and Material Properties & Volture Piezoelectric Energy Harvesters. Midé Technology Corp, Medford

Pozzi M, Zhu M (2011) Plucked piezoelectric bimorphs for energy harvesting applications. Proc SPIE 8066: 806616

Pozzi M, Almond HJA, Leighton GJT, Moriarty RJ (2015) Low-profile and wearable energy harvester based on plucked piezoelectric cantilevers. Proc SPIE 9517A: 9517061-9517069

Priya S, Inman D (ed) (2009) Energy Harvesting Technologies. Springer, New York

Roundy S et al (2005) Improving Power Output for Vibration-Based Energy Scavengers. IEEE Perv Comp 4(1): 28-36.

Taylor GW, Burns JR, Kammann SM, Powers WB, Welsh TR (2001) The Energy Harvesting Eel: A Small Subsurface Ocean/River Power Generator. IEEE J Oceanic Eng 26(4): 539-547

Techet AH, Allen JJ, Smits AJ (2002) Piezoelectric Eels for Energy Harvesting in the Ocean. Proc 12th Int Offshore & Polar Eng Conf, Kitakyushu (J)

Wang D-A, Chiu Ch-Y, Pham H-T (2012) Electromagnetic energy harvesting from vibrations induced by Kármán vortex street. Mechatronics 22(6): 746-756

Wu Y-J, Lai W-H (2010) Simulation of piezoelectric jellyfish power generator. Mod Phys Lett B24(13): 1325-1328

Zelenika S et al (2014a) Design and specification of the energy harvesters and underwater harvester anchorage. Deliverable 4.4. of the EU FP7 ICT-2009.9.1 project no. 269985 GOLDFISH, Rijeka (HR)

Zelenika S et al (2014b) Complete laboratory functionality of at least one variant of the energy harvester. Deliverable 4.5. of the EU FP7 ICT-2009.9.1 project no. 269985 GOLDFISH, Rijeka (HR)

Figure captions

Fig. 1 Considered energy harvesting concepts: hydro-generator (left), piezoelectric eel (center) and 'plucked' piezoelectric beam (right)

Fig. 2 3D model of the miniaturized hydro-generator prototype

Fig. 3 Prototypes of the 3D printed propellers with three narrow (left) and three wide blades (right)

Fig. 4 3D printed watertight enclosure (left) and assembly of the miniaturized hydro-generator prototype (right)

Fig. 5 Exploded view of the optimized hydro-generator

Fig. 6 Assembly of the executed optimized hydro-generator

Fig. 7 Dynamics of the piezoelectric eel in the furrow of the bluff body (left) and considered design parameters (right)

Fig. 8 CAD model of the piezoelectric eel (left) and corresponding silver ink electrode pattern of a single PVDF layer with four electrode pairs (on top of the PVDF layer with positive and on the bottom with negative electrodes)

Fig. 9 Manufactured eel prototype with indicated electrode segments (left) and eel's cross section (right: substrate PET layer (1), layers of electrodes and epoxy (2), PVDF layers (3) and outer protective PET layers (4))

Fig. 10 Stress-strain behavior of eel's composite material

Fig. 11 Schematics of a piezoelectric cantilever struck by a plectrum protruding radially from the shaft of a turbine

Fig. 12 FEM model of a Midé® Volture V21B scavenger (left) and corresponding impact transient response (right)

Fig. 13 Scheme of the developed power management electronics (left) and PCB with all electrical elements (right)

Fig. 14 Hydro-generator harvester in the flow channel at the Naval Research Institute in Zagreb, Croatia

Fig. 15 Measurement set-up used at the Naval Research Institute in Zagreb, Croatia

Fig. 16 Voltages generated on the hydro-generator (left) and propeller rotation speed vs. water flow velocity (right)

Fig. 17 Piezoelectric eel test bed (left) and mounting of the eel-tubular-bluff-body assembly in the flow channel (right)

Fig. 18 Quasi-sinusoidal piezoelectric eel shape when a tubular bluff body is used

Fig. 19 Voltages in eel's electrode segments for variable flow velocities and a ϕ = 200 mm tubular bluff body with d = 40 mm (left), d = 80 mm (center) and d = 120 mm (right); trend lines are shown as eel's 'pseudo shapes'

Fig. 20 Test bed for river flow measurements with a 'farm' of eels (left) and respective electrical connection diagram (right)

Fig. 21 Wireless sensor node electronics (left) and integrated underwater pollution monitoring set-up at the Liewec river, Warsaw, Poland (right)

Fig. 22 Data collected during the measurements on the integrated sensor cluster in Columbia

Table captions

Table 1 Overall requirements for the GOLDFISH sensor nodes

Table 2 DC generators used for the hydro-generator prototypes and their parameters

Table 3 Voltages at the output of the hydro-generator for two river velocities and different propeller designs

Table 4 Elements of the power management electronics

Table 5 Results of measurements performed on the miniaturized hydro-generator in the flow channel

Table 6 Characteristics of the generator-gearhead pairs adopted for the final hydro-generator solution

Table 7 Conditions during field measurements with the optimized hydro-generator harvester

Figure

Click here to download Figure Fig1.tiff

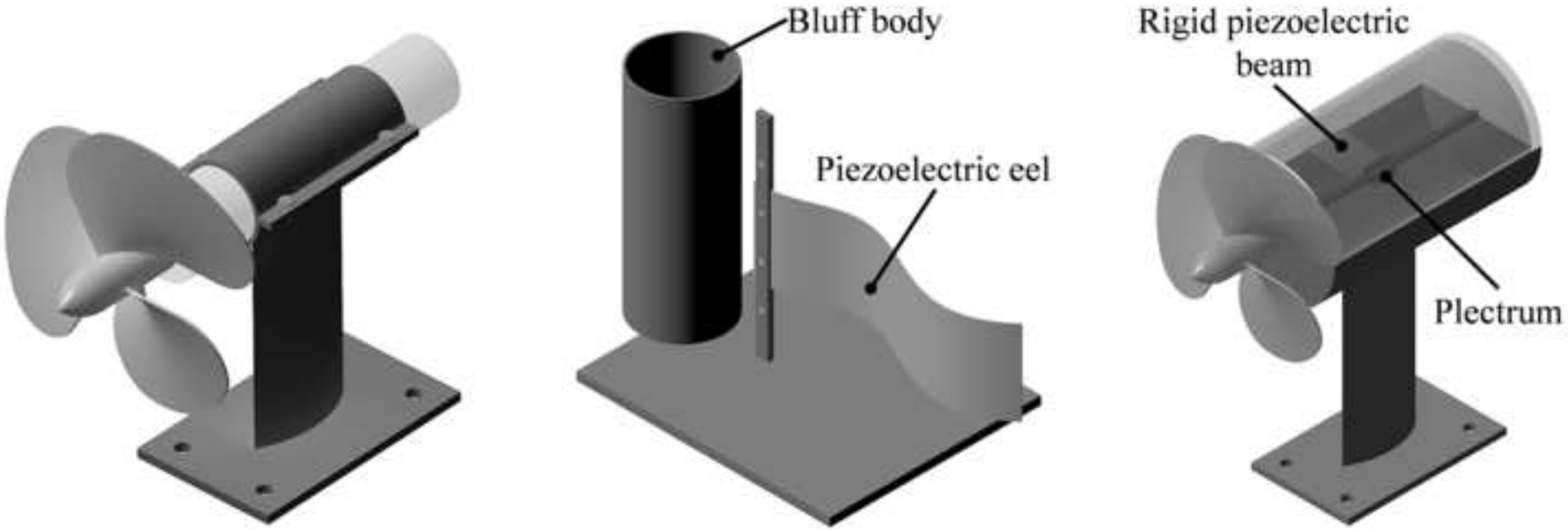

Figure

Click here to download Figure Fig2.tiff

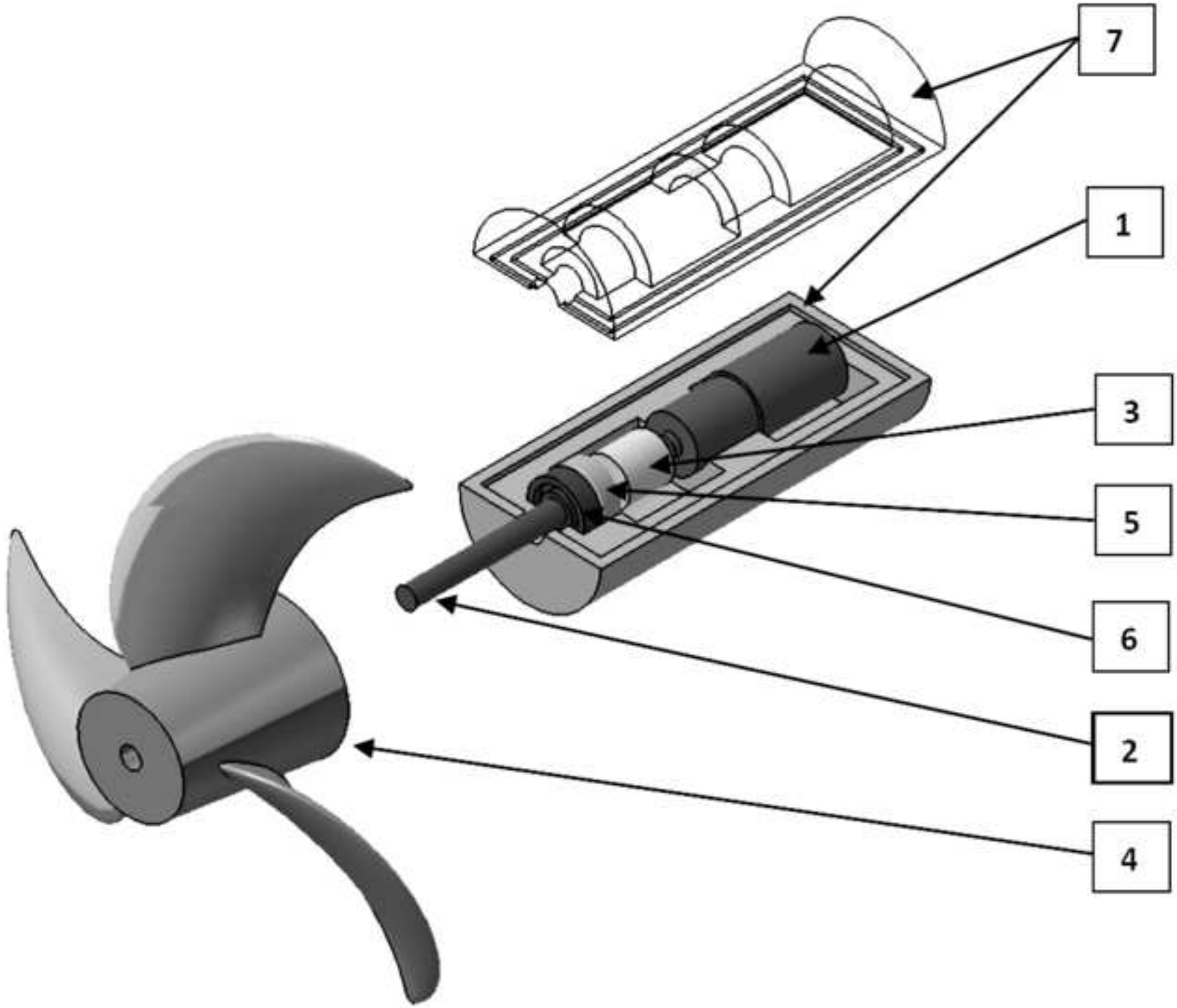

Figure

Click here to download Figure Fig3.tiff

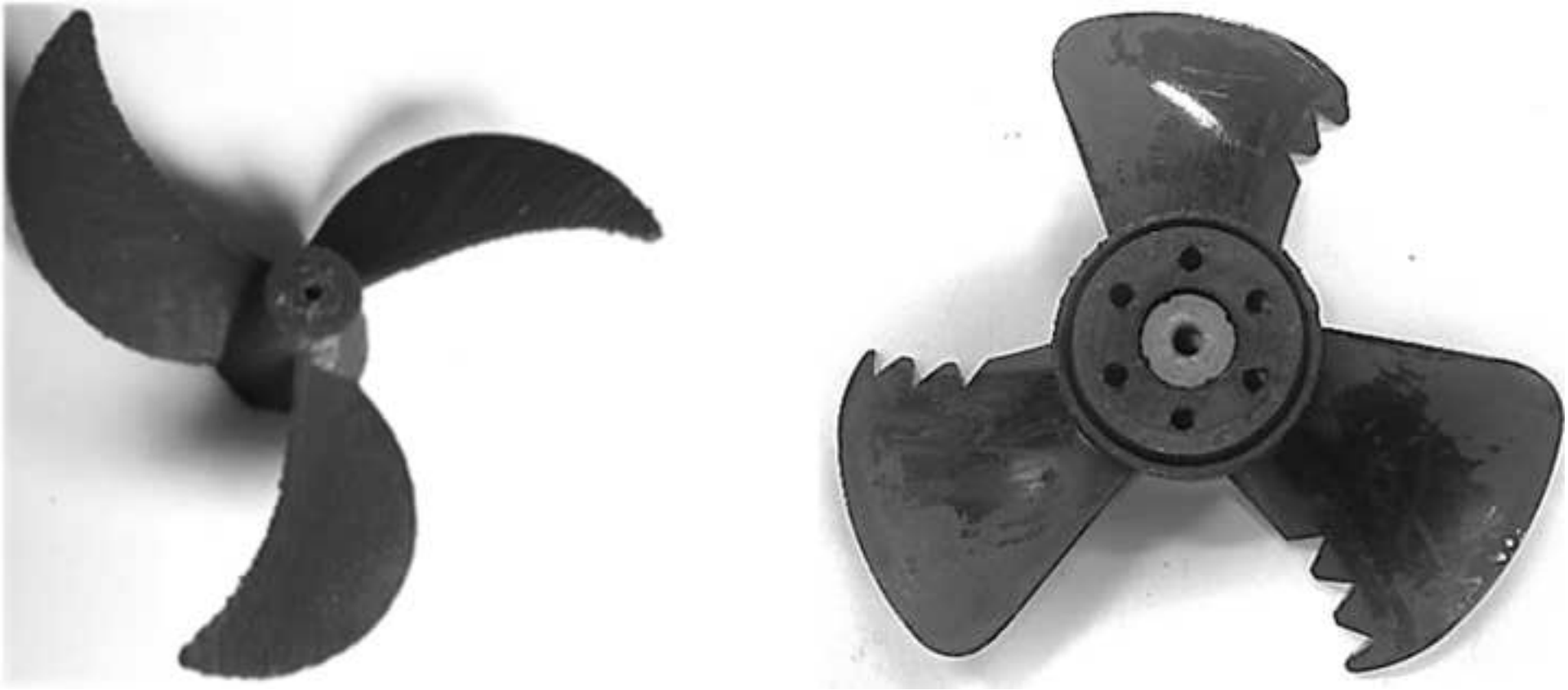

Figure

Click here to download Figure Fig4.tiff

Figure

Click here to download Figure Fig5.tiff

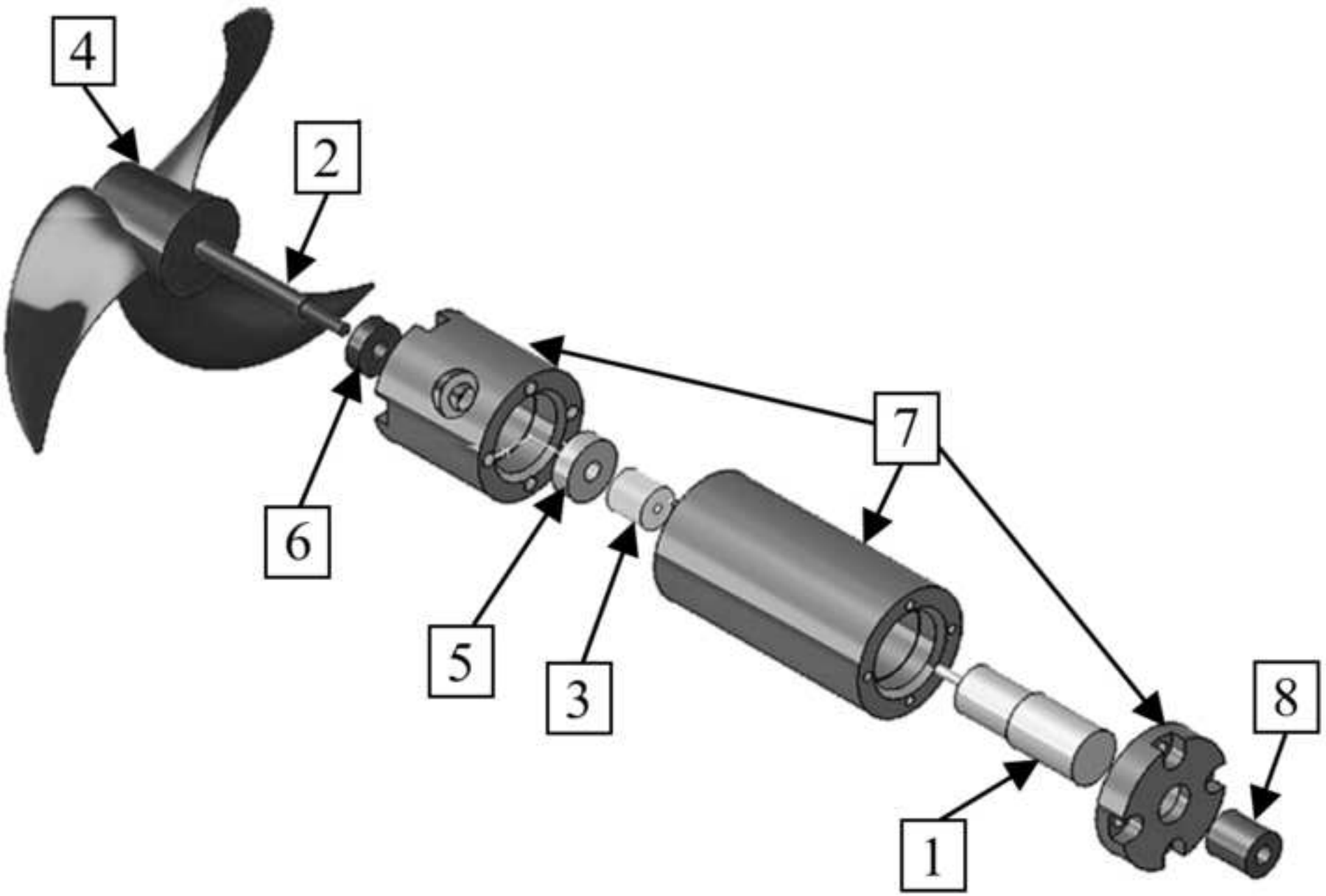

Figure

Click here to download Figure Fig6.tiff

Figure

Click here to download Figure Fig7.tiff

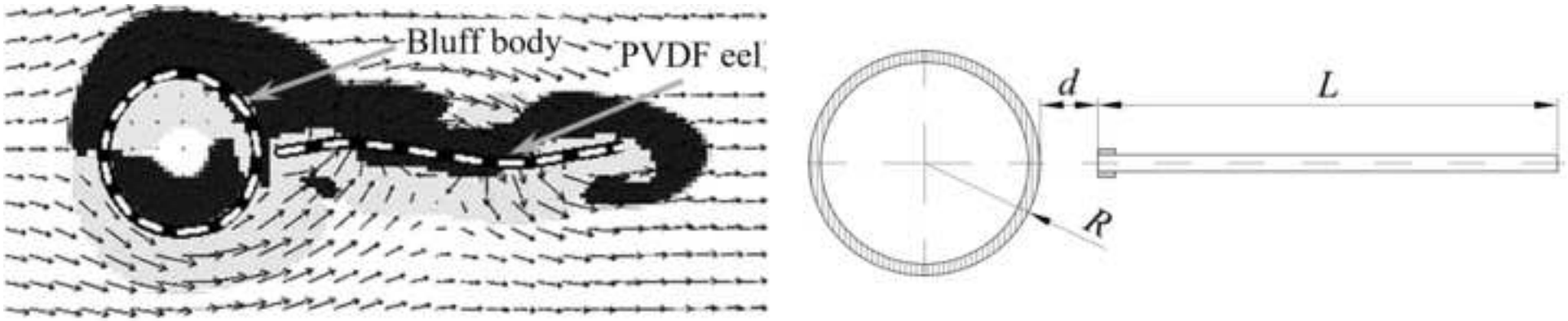

Figure

Click here to download Figure Fig8.tiff

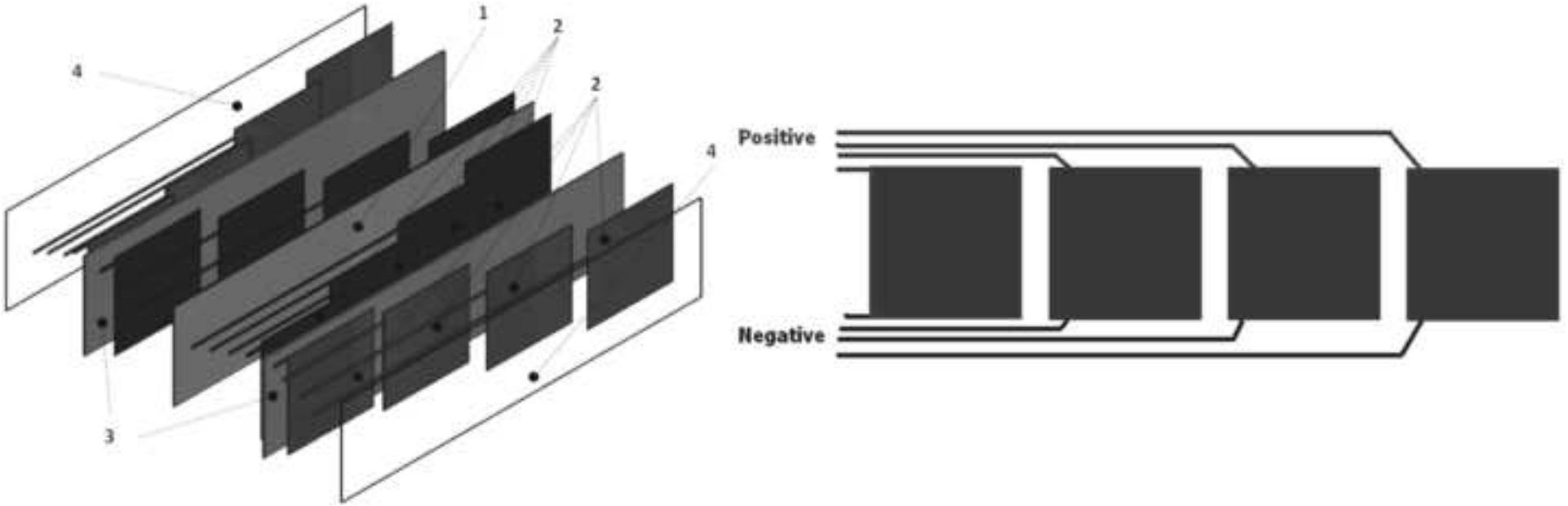

Figure

Click here to download Figure Fig9.tiff

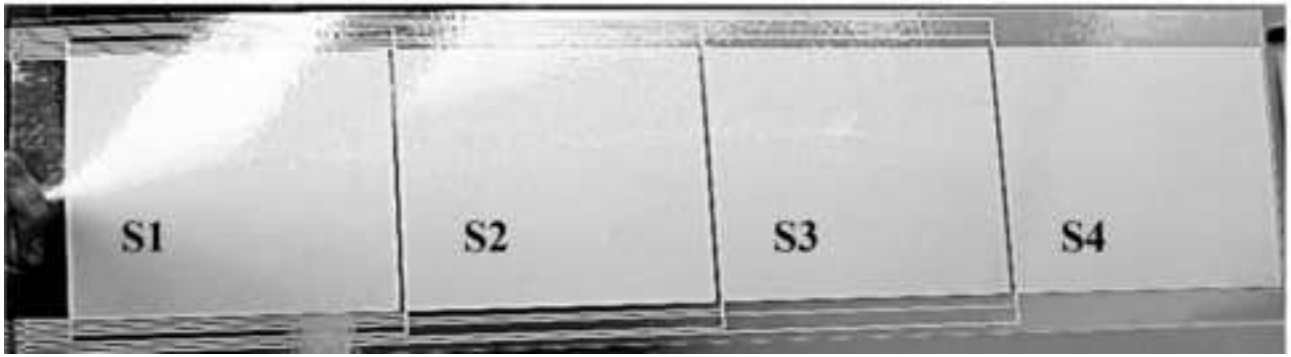

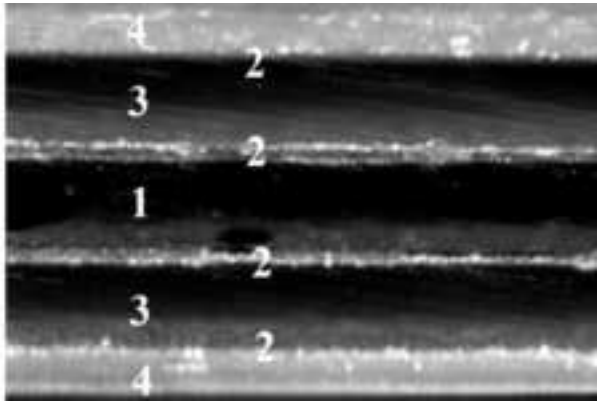

Figure

Click here to download Figure Fig10.tiff

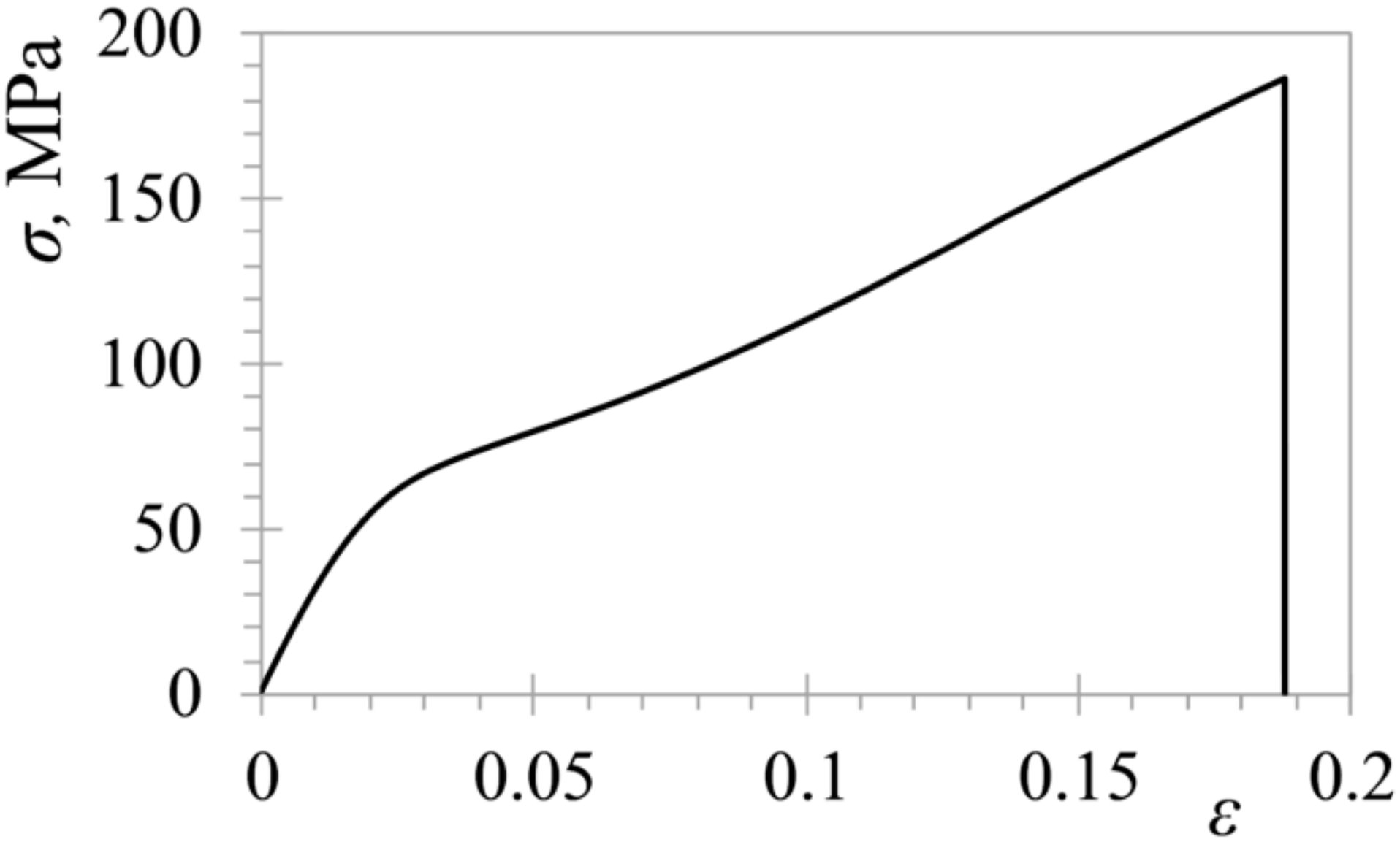

Figure

Click here to download Figure Fig11.tiff

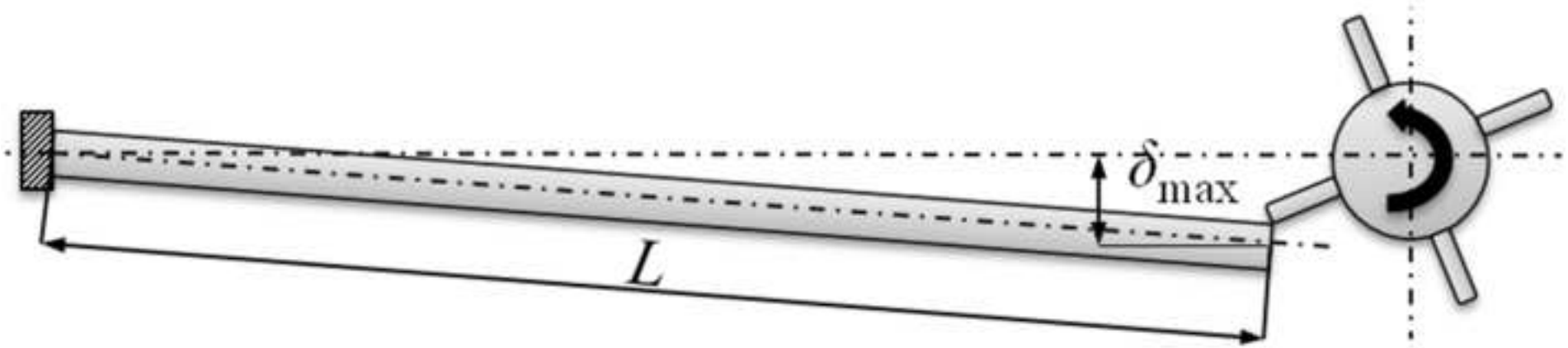

Figure

Click here to download Figure Fig12.tiff

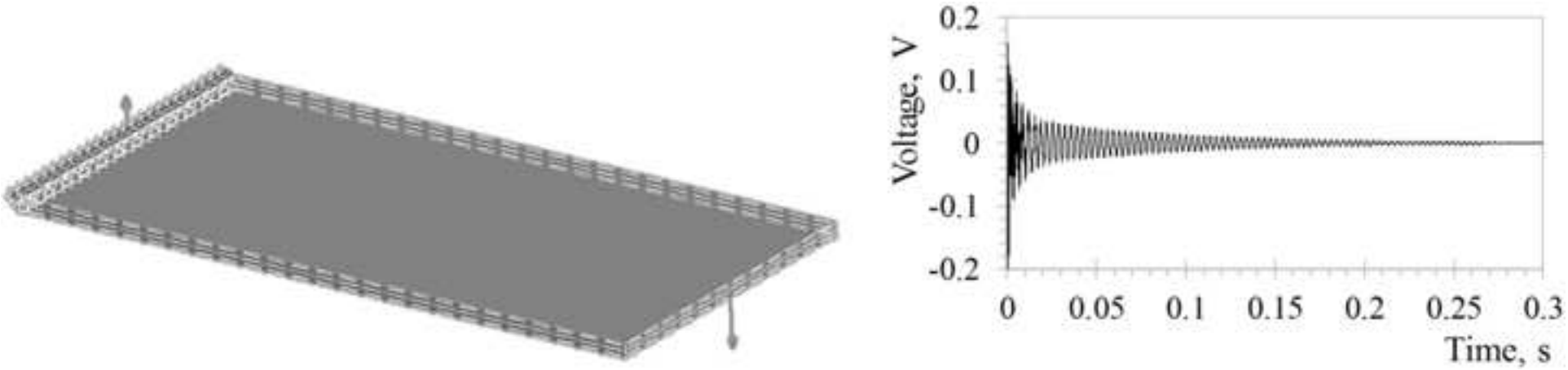

Figure

Click here to download Figure Fig13.tiff

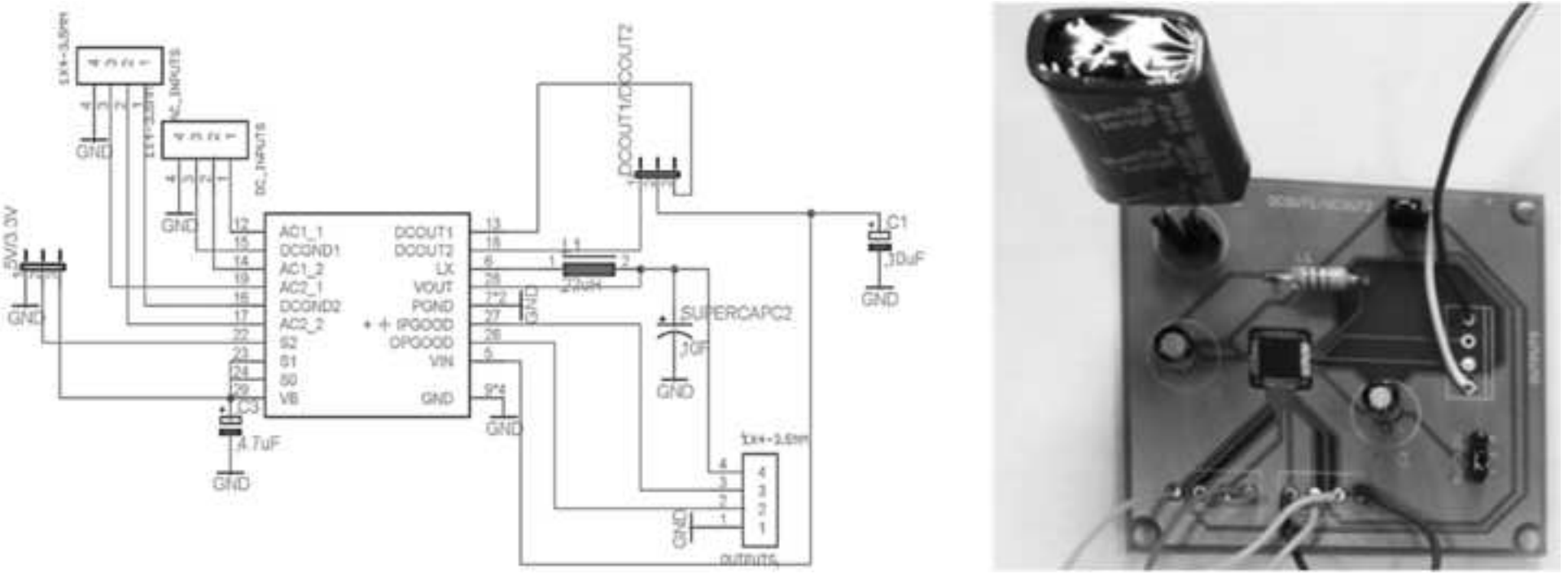

Figure

Click here to download Figure Fig14.tiff

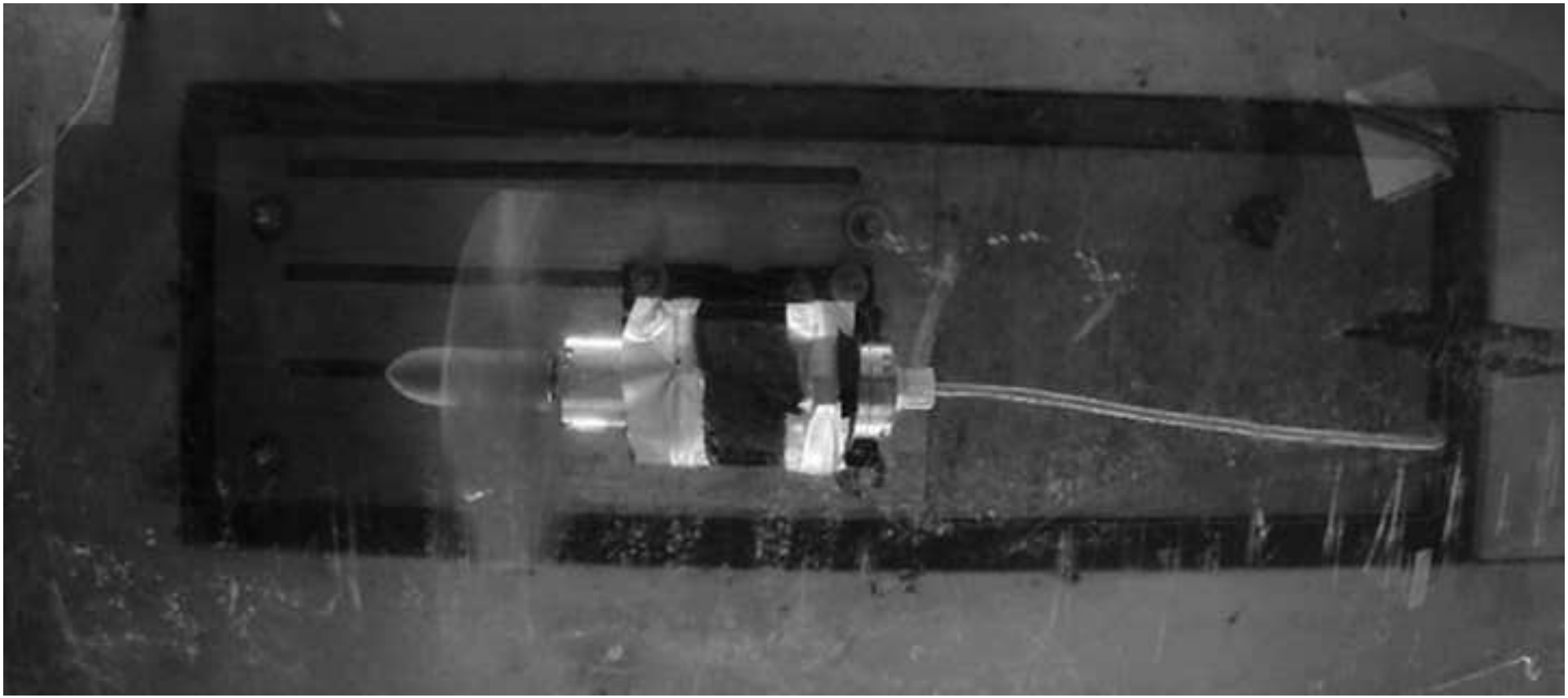

Figure

Click here to download Figure Fig15.tiff

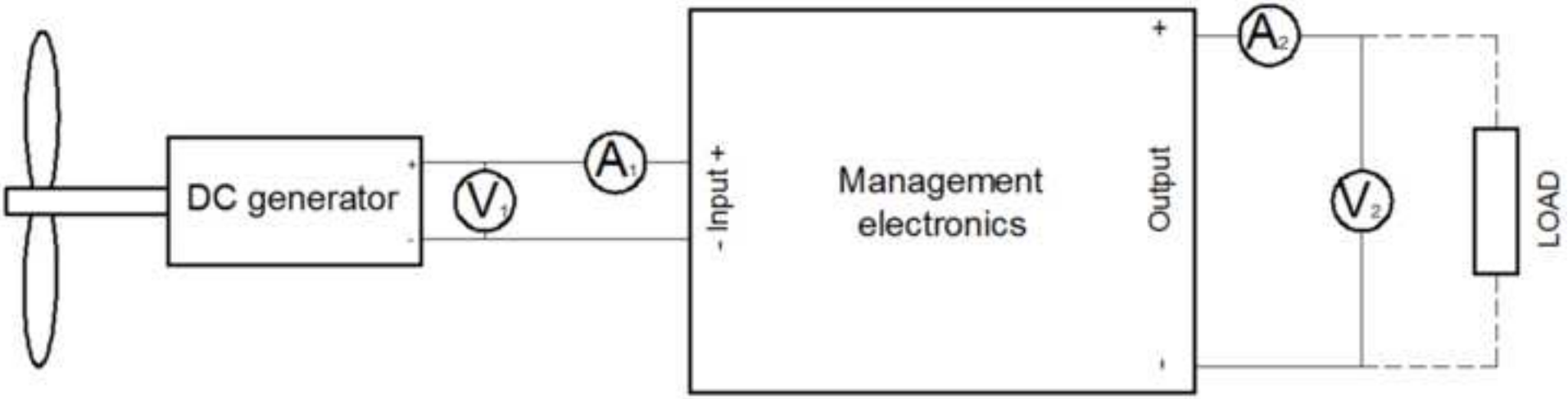

Figure

Click here to download Figure Fig16.tiff

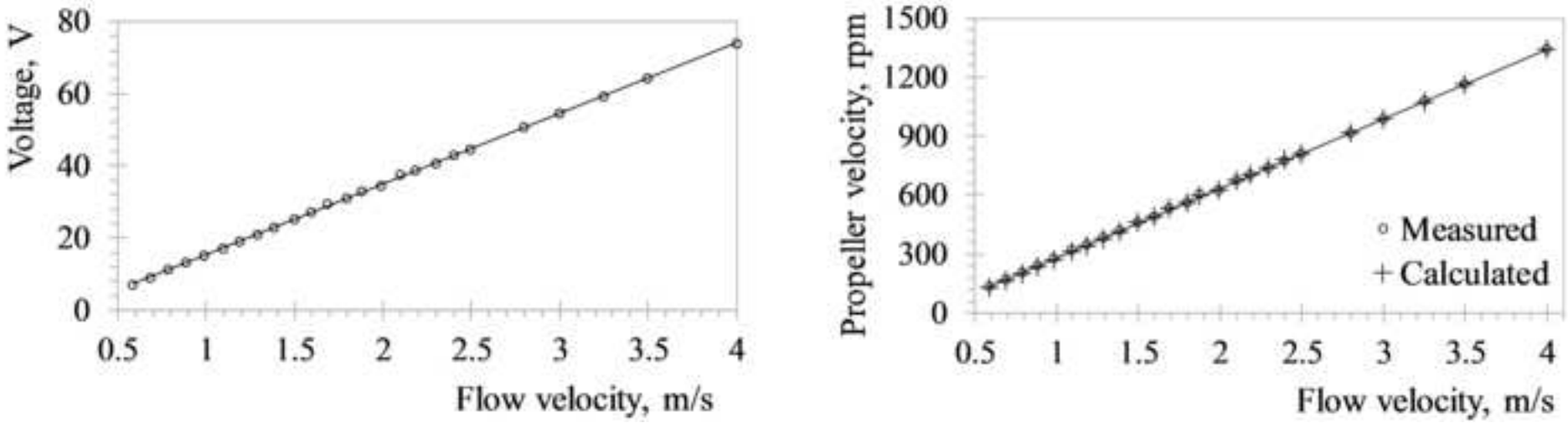

Figure

Click here to download Figure Fig17.tiff

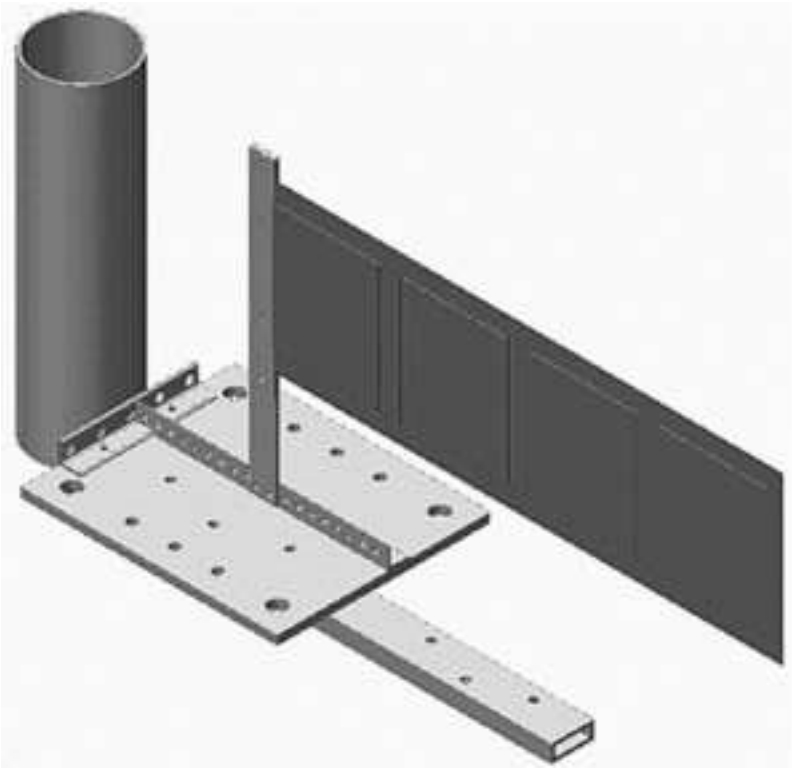

Figure

Click here to download Figure Fig18.tiff

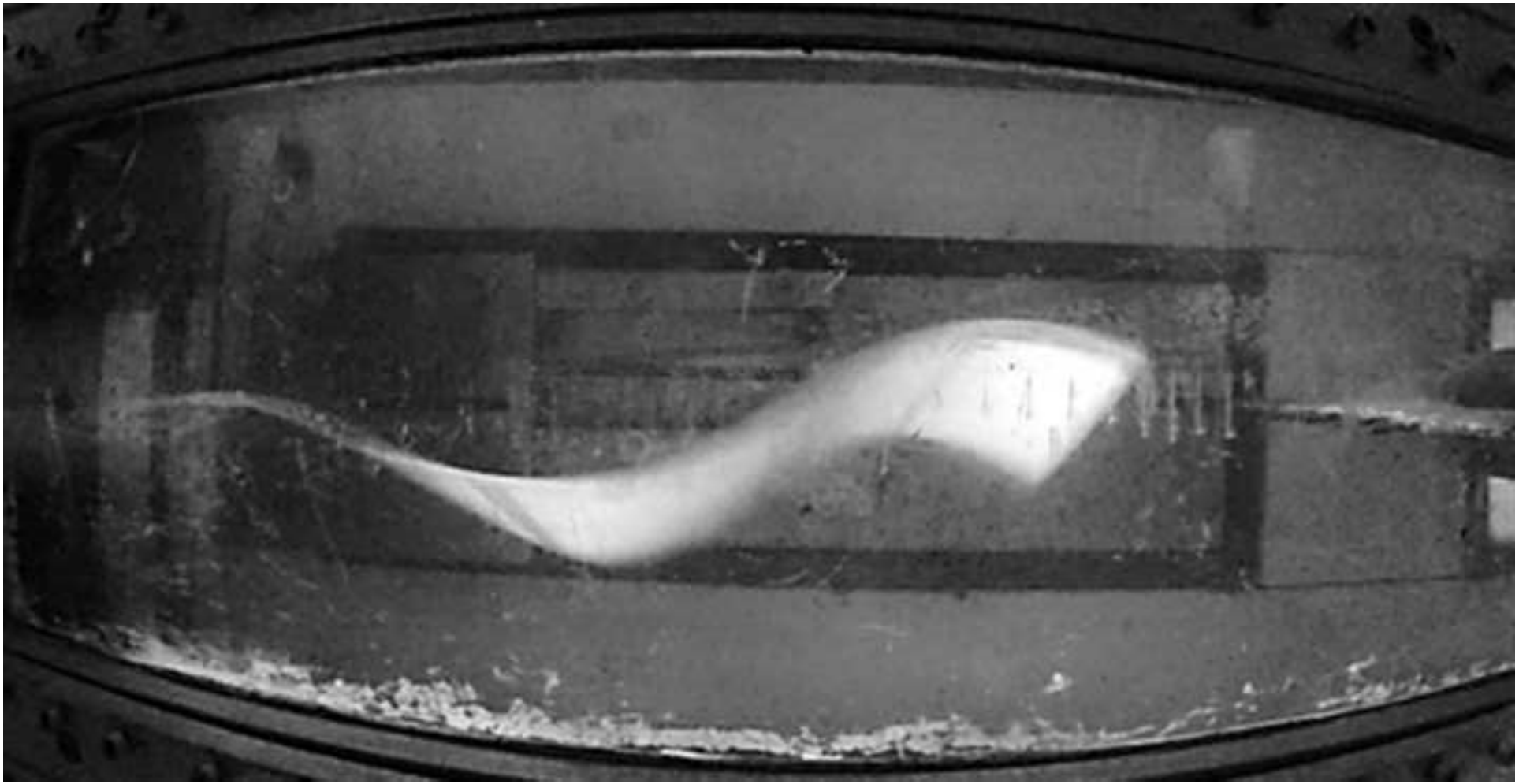

Figure

Click here to download Figure Fig19.tiff

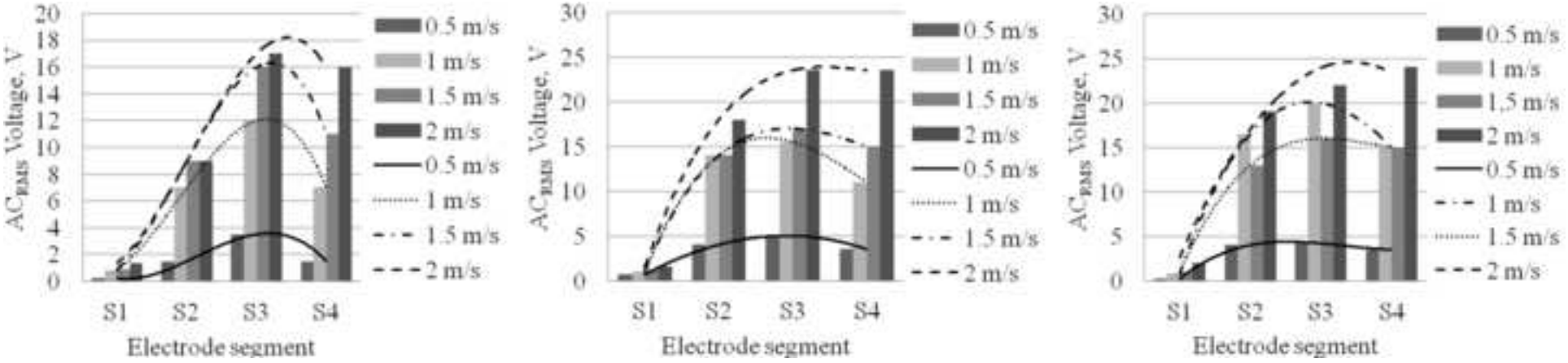

Figure

Click here to download Figure Fig20.tiff

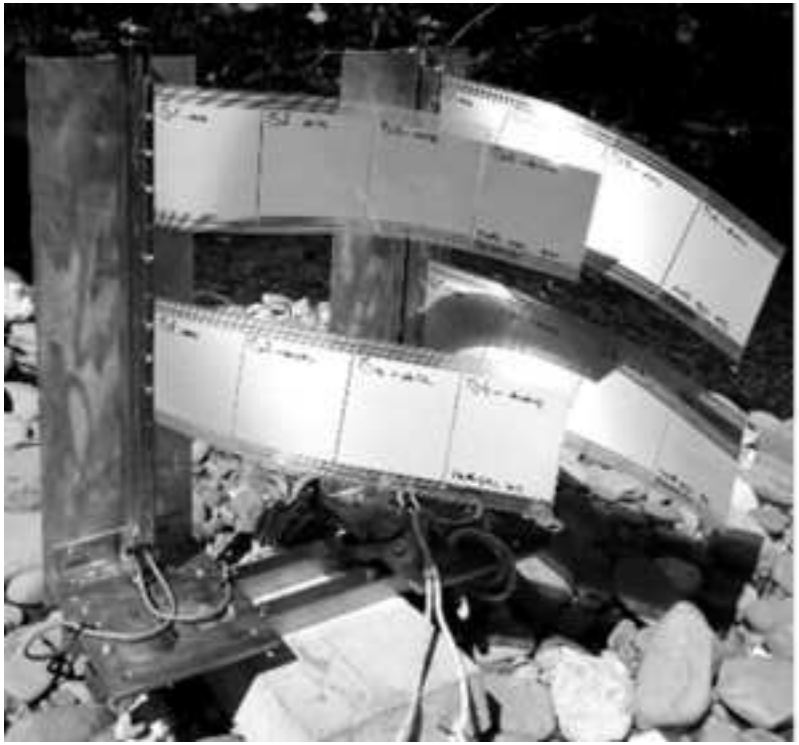

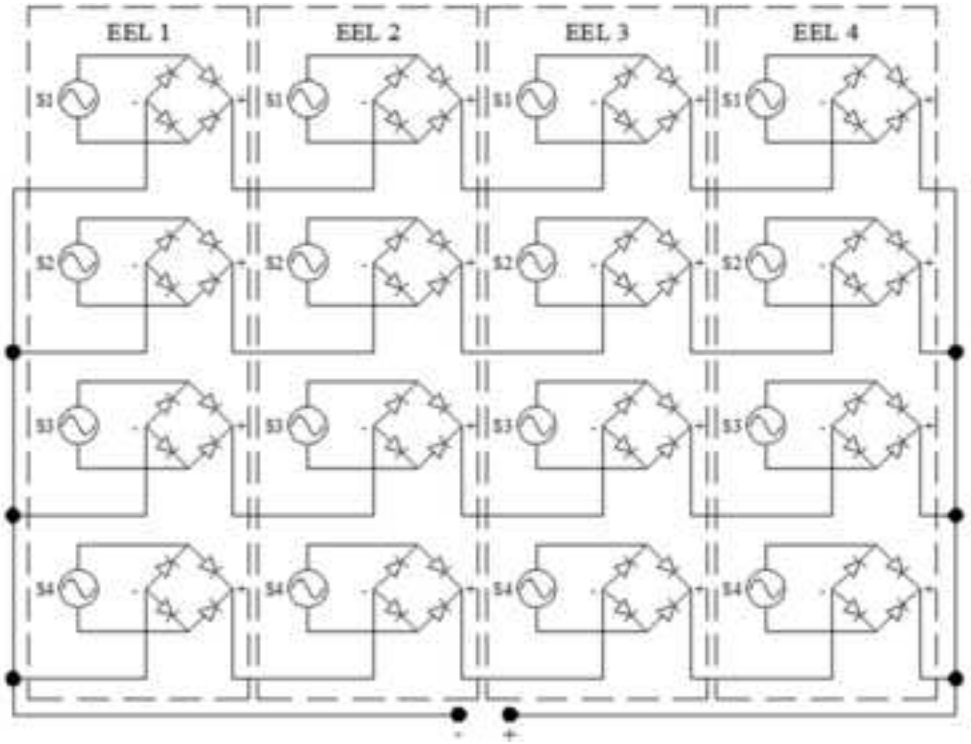

Figure

Click here to download Figure Fig21.tiff

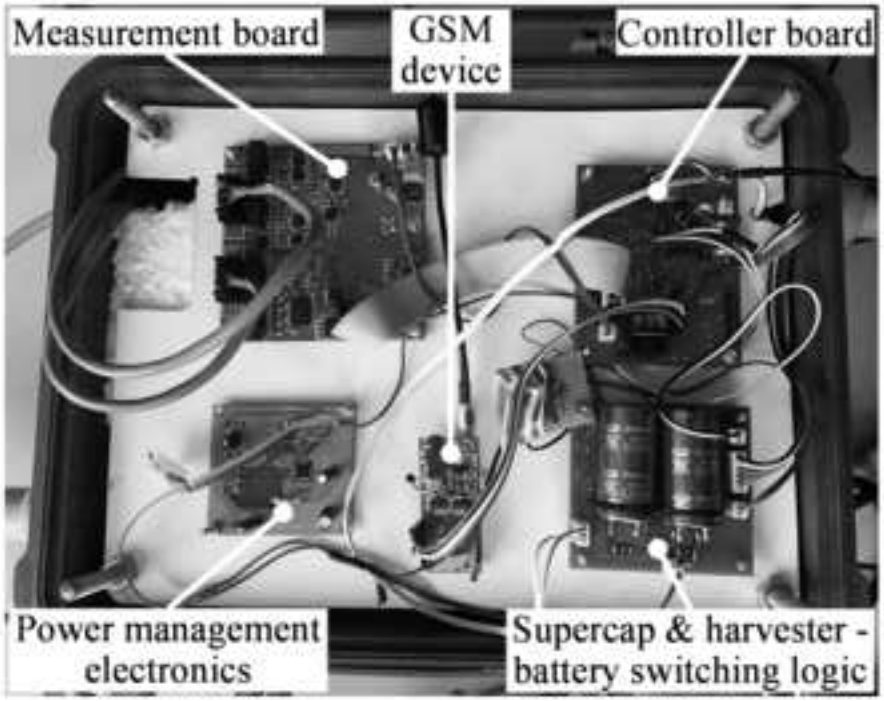

Figure

Click here to download Figure Fig22.tiff

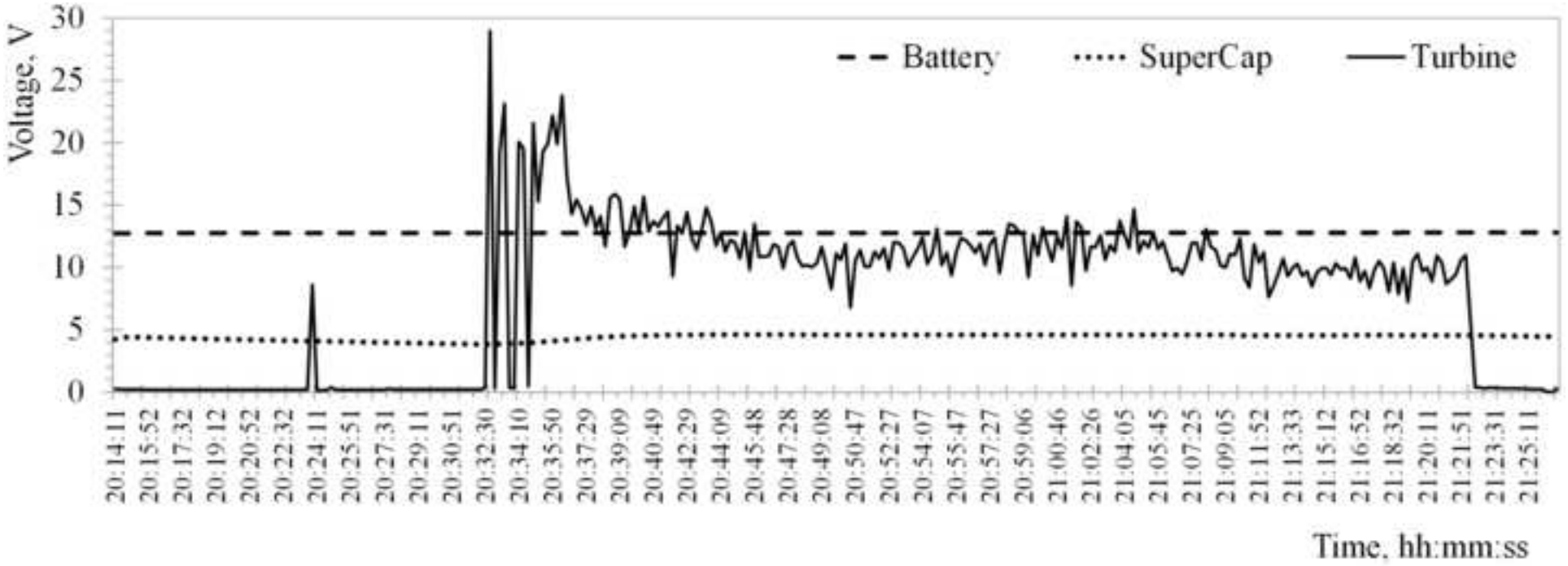

System parameter	Estimated value
River flow velocity	$0.6 < v_r < 4$ m/s
Location of sensor nodes	~ 0.5 m from riverbed, 1-6 km apart
Measurement-to-sleep duty cycle	1:15 (1 second every 15 seconds)
Data transmission rate	1:30 (2 minutes every hour)
Average power consumption of a sensor with respective measurement and controller board	100 mW (2.4 Wh/day)
Average power consumption of a sensor node with the GSM modem	500 mW (12 Wh/day)

Faulhaber device	Max voltage output, U_{max}	Power output, P_{OUT}	Velocity for max generated voltage output (before gearhead), n_0	Gearhead ratio, i	Velocity for max generated voltage (after gearhead), n_1
1724006SR	6 V	2.58 W	8600 rpm	19.2:1	448 rpm
1724012SR	12 V	2.17 W	7900 rpm	20.25:1	390 rpm

River flow velocity, v_r	Propeller type with 3 blades	Generated voltage, U_{OUT}	Average voltage, U_{OUT_av}
0.6 m/s	Narrow blades	0.8 to 1.8 V	1.3 V
1 m/s	Narrow blades	2.8 to 3.8 V	3.3 V
0.6 m/s	Wide blades	1.0 to 1.5 V	1.25 V
1 m/s	Wide blades	3.2 to 4.0 V	3.6 V

Chip	C_1	C_2 (supercapacitor)	C_3	L_1
Fujitsu MB39C811	10 μF	50 F	4.7 μF	22 μH

Flow velocity, v_r	Propeller velocity w/o load, $n_{p\_w/o}$	Propeller velocity with load, n_{p_load}	Measured/calculated no-load generated voltage, U_{no_load}	Generated voltage and current with load, U_{IN}/I_{IN}	Output voltage and current with load, U_{OUT}/I_{OUT}	Remarks about supercap charging
0.8 m/s	-	-	5.0/- V	-/-	-/-	Not charging
1.0 m/s	250 rpm	-	7.7/7.2 V	7.6 V/-	-/-	Slowly charging
1.1 m/s	293 rpm	273 rpm	9.0/8.4 V	8.3 V/33 mA	2.0 V/12.8 mA	Charging threshold at ~ 8 V
1.2 m/s	336 rpm	300 rpm	10.4 /9.7V	8.4 V/60 mA	2.0 V/12.8 mA	
1.3 m/s	377 rpm	-	11.7/10.9 V	9.9 V/49 mA	2.0 V/13.7 mA	
1.5 m/s	451 rpm	434 rpm	14.0/13.0 V	12.3 V/48 mA	2.5 V/42.0 mA	W/o load charging in 60 s
1.6 m/s	489 rpm	471 rpm	15.2/14.1 V	13.6 V/51 mA	3.0 V/72.7 mA	Stable operation

Generator model	Power output, P_{OUT}	Nominal voltage, U_n	Gearhead type and reduction ratio	Water flow velocity range, v_r
Faulhaber 2233B018S	3.19 W	18 V	22E, 28:1	0.5 … 1.0 m/s
			22E, 19:1	1.0 … 1.5 m/s
			20/1, 14:1	1.5 … 2.0 m/s
			20/1, 9.7:1	2.5 … 3.5 m/s
			20/1, 3.71:1	≥ 4.0 (… 7) m/s

River	Depth at the position of the experiment, h_1	Distance of the axis of the generator from the riverbed, h_2	River flow velocity at the axis of the generator, v_r
Rječina	0.5 m	0.3 m	~ 1.0 m/s
Liewec	~ 0.6 m	0.32 m	0.64 m/s
Coello	~ 1 m	0.35 m	1.2 m/s